Coming up short: generative network models fail to accurately capture long-range connectivity

Stuart Oldham[1,2], Alex Fornito[2] & Gareth Ball[1,3]
1. Developmental Imaging, Murdoch Children's Research Institute, The Royal Children's Hospital Melbourne
2. The Turner Institute for Brain and Mental Health, School of Psychological Sciences and Monash Biomedical Imaging, Monash University, Clayton, Australia
3. Department of Paediatrics, University of Melbourne, Melbourne

Corresponding author
Dr Stuart Oldham
Developmental Imaging,
Murdoch Children's Research Institute
Parkville 3052 VIC
Australia
stuart.oldham@mcri.edu.au

Abstract

Generative network models (GNMs) have been proposed to identify the mechanisms/constraints that shape the organisation of the connectome. These models most commonly parameterise the formation of inter-regional axonal connections using a trade-off between connection cost and some measure of topological complexity or functional value. Despite its simplicity, GNMs can generate synthetic networks that capture many topological properties of empirical brain networks. However, current models often fail to capture the spatial embedding—i.e., the topography—of many such properties, such as the anatomical location of network hubs. In this study, we investigate a diverse array of generative network model formulations and find that none can accurately capture empirical patterns of long-range connectivity. We demonstrate that the spatial embedding of long-range connections is critical in defining hub locations and that it is precisely these connections that are poorly captured by extant models. We further show how standard metrics used for model optimisation and evaluation fail to capture the true correspondence between synthetic and empirical brain networks. Overall, our findings demonstrate common failure modes of GNMs, identify why these models do not fully capture brain network organisation, and suggest ways the field can move forward to address these challenges.

Author summary

Generative network models aim to explain the organisation of connectomes using simple wiring rules. While these models replicate topological features of brain networks, they do not to capture key topographical properties, like the anatomical location of network hubs. We show that this failure occurs because the models are unable to accurately capture the spatial position of long-range inter-regional connections. Standard measures used for model evaluation also fail to accurately quantify the similarity between model and empirical networks. This study identifies how and why limitations of current generative models occur and suggests ways forward for improved practices.

Introduction

Dynamic neuronal activity coordinated across distributed brain networks supports a diverse range of complex cognitive processes. This coordination is enabled by the connectome, which comprises the complete array of white matter connections within the brain of any organism (Bullmore & Sporns, 2009). In humans, connectomes are typically studied using non-invasive diffusion magnetic resonance imaging (dMRI), which has been used to reveal a core set of complex topological properties, such as a heterogeneous distribution of connectivity across nodes (Oldham & Fornito, 2019; van den Heuvel & Sporns, 2013), small-world organization (Bassett & Bullmore, 2006, 2017), hierarchical modular architecture (Bassett et al., 2008; Meunier et al., 2009; Sporns & Betzel, 2016) and a rich-club organization in which high-degree hub nodes are strongly interconnected with each other (Arnatkevičiūtė et al., 2021; Oldham & Fornito, 2019; van den Heuvel & Sporns, 2011, 2013).

These topological properties, despite imbuing the network with a certain degree of complexity, may nonetheless arise from simple wiring principles (Albert & Barabási, 2002; Barabási & Albert, 1999; Watts & Strogatz, 1998). These principles can be studies using generative network models (GNMs), which formalize specific wiring rules which are used to construct synthetic networks (Betzel et al., 2016; Betzel & Bassett, 2017; Oldham, Fulcher, et al., 2022; Vértes et al., 2012; Vértes, 2023). Rules that give rise to networks with properties that resemble those observed in empirical data give an indication as to how connectome architecture is shaped. Therefore, generative network modelling provides a useful framework for identifying putative mechanistic or organisational principles that may underlie the formation and development of human brain networks (Betzel & Bassett, 2017; Vértes, 2023). GNMs have also been used to explore how variations in wiring rules relate to individual differences in cognitive performance and psychopathological symptoms (Akarca et al., 2021; Carozza et al., 2023; Vértes et al., 2012; Zhang et al., 2021).

Simple models that attempt to minimise the physical wiring cost of the network (often operationalized as the total connection length of the network) capture many aspects of human connectome organisation (Cherniak et al., 2004; Chklovskii, 2004; Chklovskii et al., 2002; Ercsey-Ravasz et al., 2013; Henderson & Robinson, 2013, 2014; Horvát et al., 2016;

Kaiser & Hilgetag, 2004; Raichle & Mintun, 2006; Rivera-Alba et al., 2011, 2014; Song et al., 2014), but often fail to capture properties associated with high-cost, long-range connections (Bullmore & Sporns, 2012; B. L. Chen et al., 2006; Kaiser & Hilgetag, 2006) that act as crucial foundations for dynamic brain function (Betzel & Bassett, 2018; Bullmore & Sporns, 2012; Deco et al., 2021; Kaiser & Hilgetag, 2006; Sato, 2021).

An alternative class of models that attempts to overcome the limitations of cost-only models are based on cost-value trade-offs (Bullmore & Sporns, 2012; Y. Chen et al., 2013; Schröter et al., 2017; van den Heuvel et al., 2016). These models often specify some trade-off between a penalty on long-range connections (i.e., to minimize wiring costs) and a bias towards forming connections that enhance topological complexity in some way (Akarca et al., 2021; Betzel et al., 2016; Carozza et al., 2023; Vértes et al., 2012); for caveats, see Oldham et al., 2022). Such trade-off models typically perform better than those based on cost-minimization alone, particularly when the topological bias favours a form of topological homophily, in which connections are favoured between nodes with similar neighbourhoods (Akarca et al., 2021; Arnatkevičiūtė et al., 2021; Betzel et al., 2016; Y. Chen et al., 2017; Goulas, Betzel, et al., 2019; Vértes et al., 2012; Zhang et al., 2021). Formulations incorporating wiring rules based on the molecular similarity of brain regions have also proven successful (Arnatkevičiūtė et al., 2021; Oldham, Fulcher, et al., 2022), following evidence that cortical regions with similar cytoarchitectural, molecular, and laminar organization are more likely to be connected (Barbas, 1986; Fornito et al., 2019; Hilgetag et al., 2019).

The biological insight offered by GNMs rests on their ability to accurately model empirical human brain networks. While adept at generating networks with similar topologies, GNMs generally fail to capture the way in which these properties are spatially embedded—i.e., the topography of the connectome (Akarca et al., 2021; Arnatkevičiūtė et al., 2021; Y. Chen et al., 2017; Oldham, Fulcher, et al., 2022; Zhang et al., 2021). For instance, the models can often capture the degree distribution of the empirical data, including the existence of hubs, but the hubs reside in very different anatomical locations to those of actual connectomes (Arnatkevičiūtė et al., 2021; Oldham, Fulcher, et al., 2022). This oversight is critical given that the brain's geometry constrains its function (Pang et al., 2023), and cortical hubs are positioned to achieve a near-optimal trade-off between wiring costs minimization and

promoting complex, efficient brain dynamics (Gollo et al., 2018; Roberts et al., 2016). Topographical properties of the brain thus represent important features that generative models of brain networks should capture.

In this study, we perform a comprehensive evaluation of the ability of GNMs to reproduce both the topology and topography of human brain networks. We identify common failure modes across model formulations and demonstrate how and why synthetic networks generated by GNMs fail to capture critical properties of empirical human brain networks.

Results

Generative models of the human connectome

We defined GNMs using a standard formulation (Betzel et al., 2016; Oldham, Fulcher, et al., 2022). Given a network of n nodes, the models add connections sequentially to populate an empty $n \times n$ adjacency matrix, A, according to the wiring-rule

$$w_{ij} = f(D_{ij}) + f(F_{ij}), \quad (1)$$

wherein the probability of adding a connection at each step is given by a function, f, of wiring distance between a pair of nodes, D_{ij}, and a function of the topological property of that node pair, F_{ij} (**Figure 1A,B; Methods;** alternative formulations were explored in supplementary analyses). The parameters of the model were formulated to always impose a penalty of long-range connections (the strength of which could vary), while affording the flexibility to form connections between regions with similar or dissimilar nodal properties (Oldham, Fulcher, et al., 2022). We defined a total of 10 different GNMs (**Table 1**), which included: one where pairwise similarities between nodes F_{ij} was defined using the matching index, which quantifies the similarity of the topological neighbourhoods between nodes ((Betzel et al., 2016); *Matching*); seven with similarity defined by different cortical features, which include similarity in gene expression, receptor density, lamination, glucose uptake, haemodynamic activity, electrophysiological activity, and temporal profiles (Hansen et al., 2023); and two baseline models, one using wiring distance only (*Spatial*); and one where

nodal similarity was based on random, spatially autocorrelated data (*Random similarity*). In supplementary analyses, we examined an additional 11 topological GNMs (**Table S1**).

Table 1
Description of different generative network models

GNM	Description of wiring rule
Spatial	Spatial distance between regions (i.e., wiring cost)
Gene co-expression	Regional similarity in gene expression combined with a wiring cost
Receptor similarity	Regional similarity in receptor density combined with a wiring cost
Laminar similarity	Regional similarity in cortical layer histology combined with a wiring cost
Metabolic coupling	Regional similarity in PET timeseries combined with a wiring cost
Haemodynamic coupling	Regional similarity in fMRI timeseries combined with a wiring cost
Electrophysiological coupling	Regional similarity in MEG timeseries combined with a wiring cost
Temporal similarity	Regional similarity in fMRI timeseries features combined with a wiring cost
Random similarity	Regional similarity in randomly generated spatially autocorrelated features combined with a wiring cost
Matching	Regional similarity in topological neighborhoods combined with a wiring cost

Synthetic networks generated by each GNM were compared to a consensus 200 region left hemisphere network, constructed using diffusion tractography from 326 unrelated participants of the Human Connectome Project (Hansen et al., 2023). Topological similarity between model and empirical connectomes was assessed via the $max(KS)$ statistic – which is the maximum Kolmogorov-Smirnov (KS) statistic between the node degree, node betweenness, node clustering, and connection length cumulative distribution functions for a pair of networks (**Figure 1C**; see **Methods**). Model parameters were fitted by optimizing the $max(KS)$ statistic. Topographical similarity was measured by connection recovery (*R*), defined as the proportion of empirical connections that the model network successfully recaptured, and the correlation between model and empirical network's nodal degree (**Methods**).

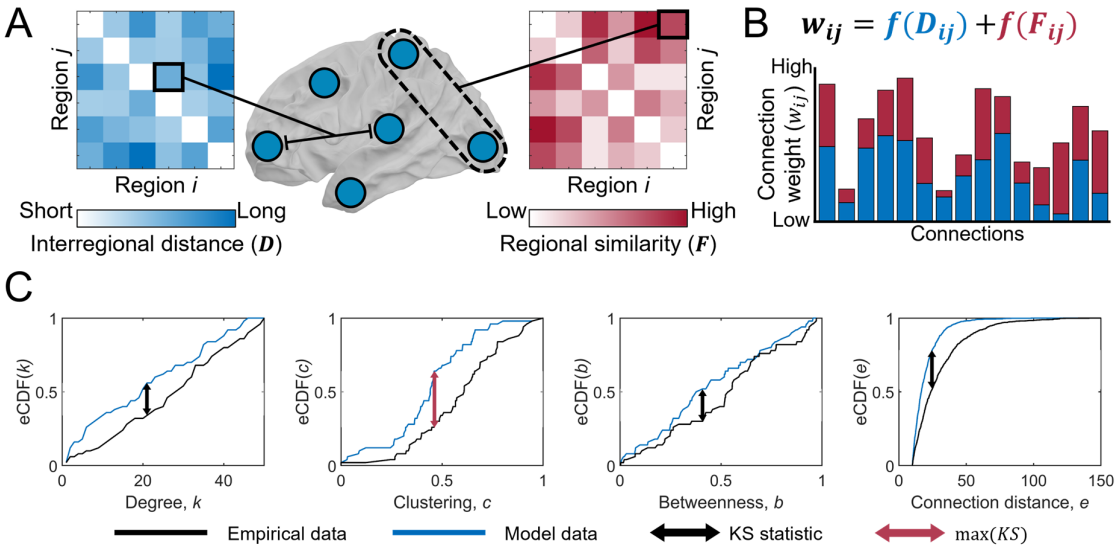

Figure 1. Schematic of the generative network model and $\max(KS)$ calculation. (A) The distance (wiring cost; D_{ij}) and topological similarity for a given feature (F_{ij}) between nodes i and j is used in the generative network model. **(B)** Each connection is assigned a weight: $w_{ij} = f(D_{ij}) + f(F_{ij})$, where $f(x)$ indicates a normalisation/weighting function. The model adds connections on an iterative basis to a network based on w_{ij} (higher values indicate a greater likelihood of forming, bar plot). **(C)** Topological similarity between empirical and synthetic networks is defined as the maximum Kolmogorov–Smirnov (KS) statistic $\max(KS)$ across four topological distributions: degree, clustering, betweenness, and connection distance. The arrows indicate where the KS statistic is calculated; the red arrow indicates the maximal difference across the four properties (i.e., $\max(KS)$).

GNMs capture topological, but not topographical properties of empirical networks

The best fit to empirical network topology, indicated by lowest $\max(KS)$, was achieved by models based on temporal ($M = 0.159$, $SD = 0.016$), laminar ($M = 0.172$, $SD = 0.015$), and random node similarity ($M = 0.181$, $SD = 0.01$; **Figure 2A, B**). All models achieved mean $\max(KS)$ < 0.4, with values closer to 0 indicating a greater topological fit (**Figure 2**).

Despite this reasonable performance in capturing network topology, the mean connection overlap between empirical and synthetic networks ranged between only 32% and 42% across all GNM formulations (**Figure 2A**). Thus, most connections in the model are between node pairs that are not connected in the empirical data. Similar performance was observed across alternative GNM formulations (**Figure S1-S2**). Poor correspondence between empirical and synthetic connections resulted in low rank correlations between the node degree sequences (i.e., the degree topography) of the model and empirical data (i.e., -0.50 < *r* < 0.18; **Figure 2B-C**; **Figure S1-S2**).

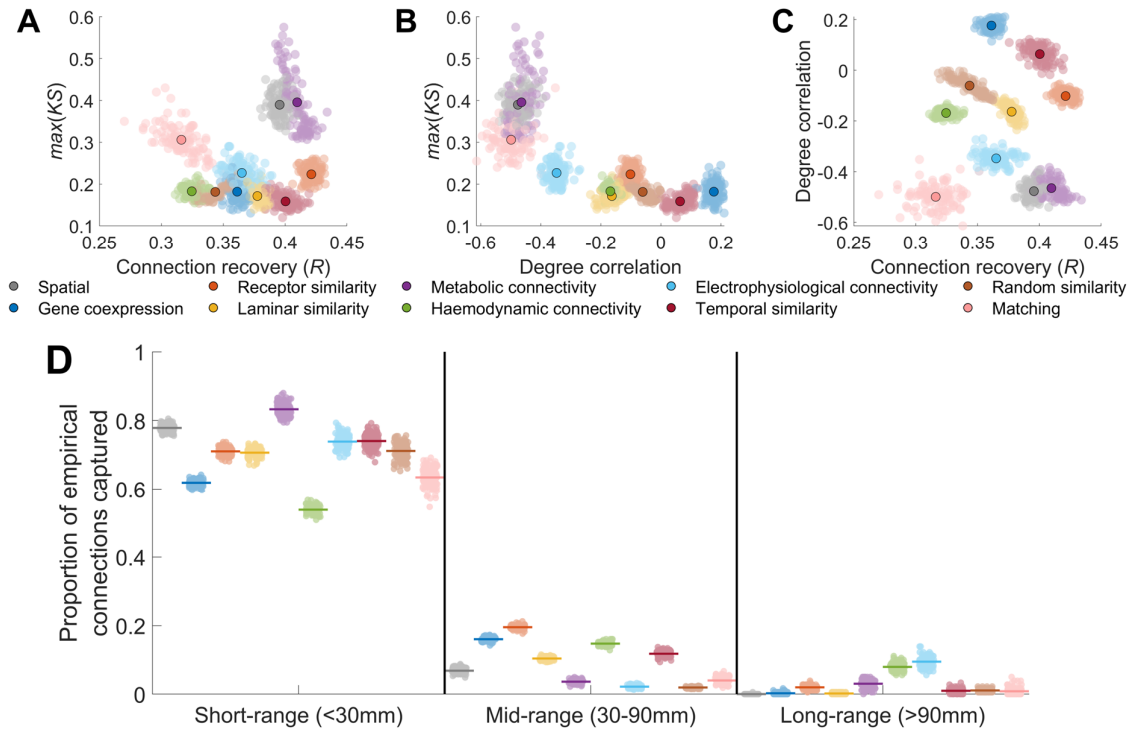

Figure 2. Performance of generative network models in capturing topological and topographical properties **(A)** Relationship between $\max(KS)$ and connection recovery of synthetic model networks. **(B)** Relationship between $\max(KS)$ and the correlation between empirical and model node degree. **(C)** Relationship between connection recovery and the correlation between empirical and model degree. In each plot, the outlined point indicates the average across model runs for different model formulations (**D**) Proportion of empirical short-range, mid-range, and long-range connections captured by the best fitting generative network models. The coloured line indicates the average overlap, while each point indicates the result for an individual model network.

Overall, the overlap between empirical network and GNM network connections was low. We observed a clear distance-dependence of connection recovery, with the recovery of short-range connections considerably higher (51-84% of empirical connections <30mm), dropping to 2-20% for mid-range (30-90mm) and 0-10% for long-range (>90mm) connections (**Figure 2B**; **Figure S3-S4**). These findings suggest that GNMs can produce synthetic network with similar topological properties to empirical connections but fail to accurately model long-range connections, leading to poor topographical correspondence between model and data.

To demonstrate the importance of long-range connections in defining the degree topography of the network, we applied a length threshold to the empirical network and then iteratively added longer connections. At each iteration, we compared the degree sequence with the original unthresholded network. When retaining only short connections

only (<30mm), nodal degree was only weakly correlated with the full network (r = 0.23). The addition of longer connections led to increasingly highly correlated degree sequences (**Figure 3**). In contrast, removing all short-range connections below 60mm from the empirical network largely preserved degree sequence (**Figure S5**), indicating that the spatial embedding of node degree is largely driven long-range connectivity between hub nodes. These results indicate that long range connections, despite only making up the minority of connections (e.g., connections >60mm only make up 26% of all connections), are vital to defining the degree topography of the cortex.

We repeated this analysis using GNMs with parameters chosen to maximise the degree sequence correlation, and therefore topographical overlap, with empirical networks (rather than minimise $\max(KS)$). This analysis resulted in similar findings: synthetic networks produced by these models had a degree correlation of ~ 0.3, but only captured a maximum 25% of empirical connections (**Figure S6**), with an overall failure to capture long-range connections (**Figure S7**).

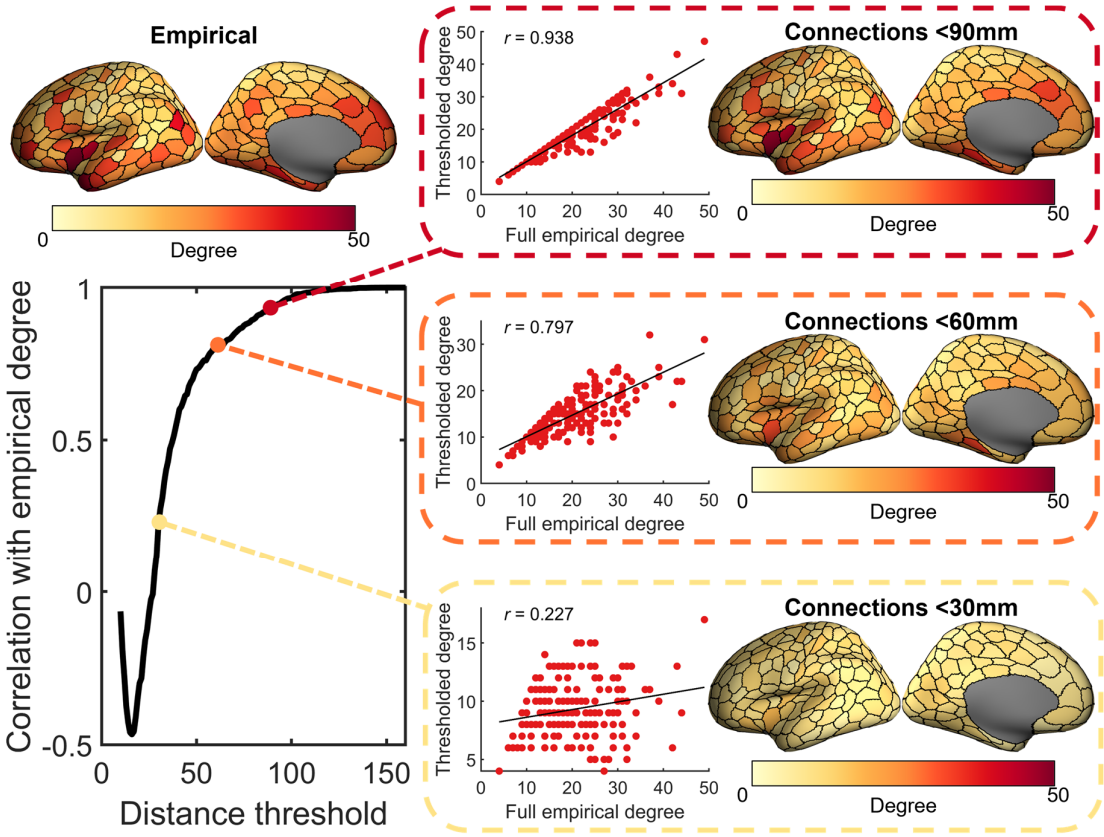

Figure 3. Similarity of the empirical degree sequence at different distance thresholds. Degree is calculated only using connections with a length less than the current distance threshold. The thresholded degree is then correlated with the full empirical degree (i.e., degree calculated when using all empirical connections). Degree is largely shaped by connections >30mm (particularly mid-range connections), meaning that these specific connections need to be captured to obtain the empirical spatial embedding of nodal degree.

To determine why GNMs do not accurately model long-range connections between hub nodes, we calculated the probability of each connection (P_{ij}) during model fitting as a function of connection length. In all models, P_{ij} was negatively associated with connection length (**Figure 4A; Figure S8**). While at short distances, almost all edges assigned high probability by the model are connected in the empirical networks, at longer ranges only a small proportion of high probability edges are connected (**Figure 4B**). At connection lengths over 60mm, only 6% of the top 25% most probable connections exist in the empirical data across all GNMs, a similar proportion to that expected by selecting edges at random (**Figure 4B**). As such, GNMs are highly unlikely to accurately identify the long-range connections between empirical hub nodes (**Figure S9**).

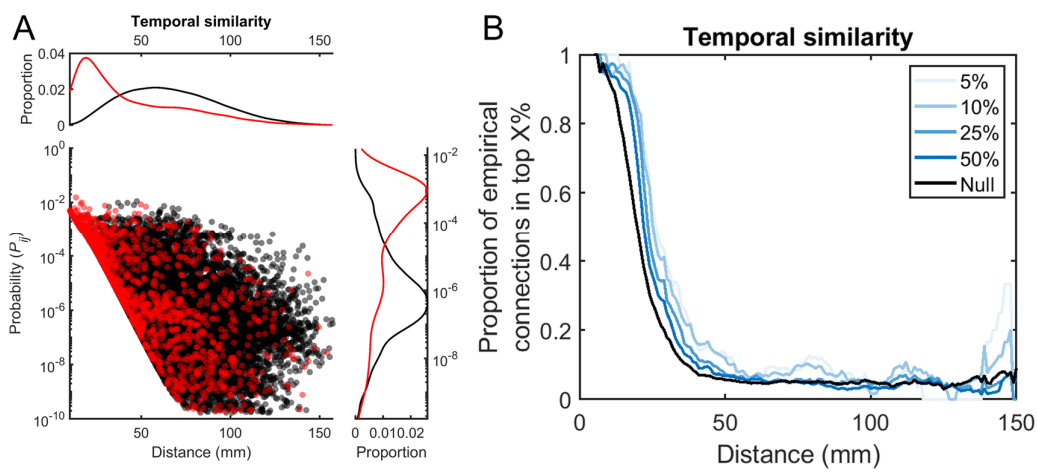

Figure 4. Connection probabilities of the model with the lowest $\max(KS)$. (A) Connection probabilities for the temporal similarity generative network model. The connection probabilities are the mean probability assigned to each connection across all steps of the model. Red points indicate empirical connections (i.e., connections that exist in the empirical data) while black points indicate empirical non-connections (i.e., connections that do not exist in the empirical data). Kernal density plots for the structural and non-structural connections are shown for the distributions of distance/length and probability against the respective axis. **(B)** Most probable connections at different distances. Using a sliding window analysis, at each distance (±5mm) the top X% of connections with the highest probability are found. The proportion of these which are empirical connections is then calculated. The "null" line indicates the proportion of empirical structural connections that exist at that distance (i.e., the probability of selecting an empirical structural connection if all connections at a given distance were equally probable).

The $\max(KS)$ fit statistic can obscure important differences in network structure

Our results have demonstrated that maximising topological similarity between two networks through minimisation of the $\max(KS)$ statistic can result in widely different network topographies and poor correspondence between empirical and synthetic network connections (**Figure 2A-C**). We next sought to understand how variations in the $\max(KS)$ statistic relates to topological and topographical variations across networks. To assess this relationship systematically, we analysed the consensus empirical human brain network by rewiring its connections one at a time, either at random or based on connection length (see **Methods**), and computing $\max(KS)$ between the rewired and original networks (**Figure 5**).

We observed that $\max(KS)$ increased rapidly as connections were rewired (**Figure 5A**), such that rewiring of just 62 connections resulted in a $\max(KS)$ of 0.16 with 97% of empirical connections retained (**Figure 5A**). This value is comparable to the $\max(KS)$ of the best performing GNMs (**Figure 2**), which only replicated, at most, 40% of connections. Constraining the algorithm to only rewire long connections, thus leaving shorter connections in place, reduced this effect with $\max(KS)$ most sensitive to changes in shorter connections (**Figure 5A**). When we examined how the correlation between the nodal degree of the original and rewired network varied across iterations, we found that rewiring long-range connections caused a greater decrease in the correlation than rewiring short-range connections (**Figure S10**).

The $\max(KS)$ statistic is a composite of four different topological properties (degree, clustering, betweenness, connection length; **Figure 1**). Examining the KS statistic for each of these four properties, we found that the increased $\max(KS)$ largely reflected changes in the network clustering coefficient (**Figure 5B-E**). The rewiring analysis indicates $\max(KS)$ is highly sensitive to small perturbations in network connectivity that disrupt network clustering.

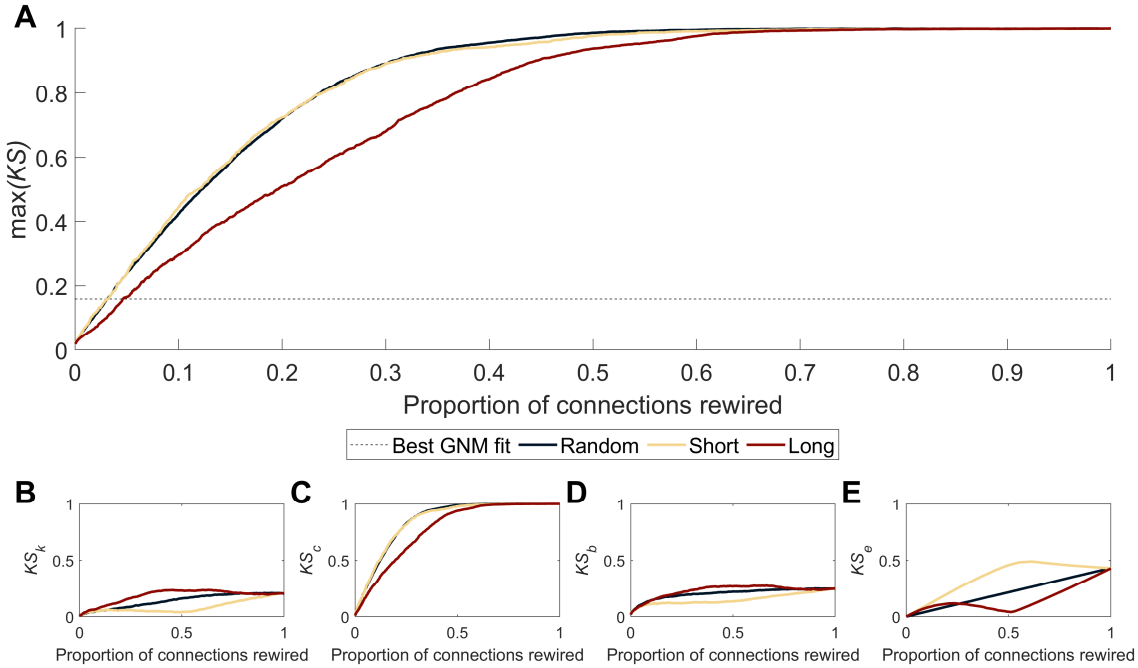

Figure 5. Effect of iteratively rewiring connections on $\max(KS)$. (A) The proportion of connections rewired and its effect of $\max(KS)$ for different rewiring algorithms. The *random* algorithm rewired connections at random but of a similar length; *short* rewired connections from shortest to longest connections with those of a similar length and; *long* rewired connections from longest to shortest connections with those of a similar length. The dotted line indicates the lowest $\max(KS)$ fit obtained in the GNMs. Plots also show the change in the KS statistics for the degree **(B)**, clustering **(C)**, betweenness **(D)**, and connection length **(E)** distributions (KS_k, KS_c, KS_b, and KS_e respectfully). Changes in $\max(KS)$ were almost exclusively driven by changes in clustering.

While the pattern of topological and topographical features is relatively conserved across individual empirical brain networks, there is still individual variation. To establish how this variation is reflected in variations of the $\max(KS)$ statistics in empirical connectomes, we compared 972 individual networks constructed from Human Connectome Project data, using 10 parcellations (Schaefer 100 to 1000) and deterministic or probabilistic tractography (see **Methods**). All networks produced using a given parcellation and tractography algorithm were matched for the same density. We fitted the 10 GNM types to the ensemble of individual empirical networks generated with the Schaefer 400 parcellation. For each individual, we a) identified the synthetic network with the lowest $\max(KS)$ value and b) calculated the $\max(KS)$ with respect to every other empirical network as well.

We found that the similarity between empirical brain networks, as measured by the $\max(KS)$ statistic, varied depending on parcellation size, with finer parcellations showing greater consistency across individuals (**Figure 6**). Overall, $\max(KS)$ varied from 0.035 to

0.325 between individual empirical network pairs, with connection overlaps ranging from ~30 to >85%.

Both topological and topographical similarity varied with parcellation resolution. For example, the Schaefer 100 parcellation had a mean $\max(KS)$ of 0.15 (SD = 0.039) compared to the Schaefer 400 parcellation (0.09, SD = 0.028) and the Schaefer 1000 parcellation (0.070, SD = 0.022). Empirical networks created using coarser parcellations also showed greater connection overlap between individuals (e.g., Schaefer 100: *M* = 0.752, SD = 0.025; Schaefer 400: *M* = 0.571, SD = 0.024; Schaefer 1000: *M* = 0.435, SD = 0.021), in addition to higher degree correlations (e.g., Schaefer 100: *M* = 0.786, SD = 0.058; Schaefer 400: *M* = 0.710, SD = 0.047; Schaefer 1000: *M* = 0.63, SD = 0.043), than finer resolution parcellations (**Figure 6**). Similar results were obtained when using deterministic tractography (**Figure S11**).

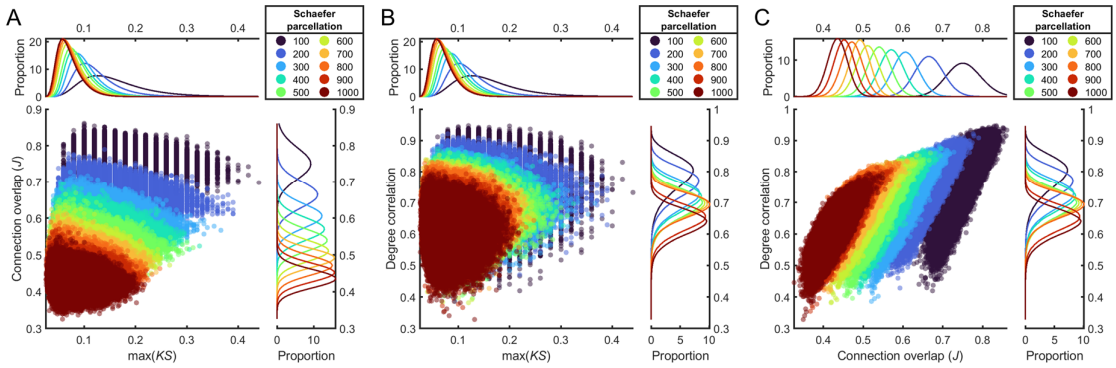

Figure 6. Performance of $max(KS)$, connection overlap, and similarity of the degree distribution when comparing empirical networks produced using probabilistic tractography. (A) Relationship between $max(KS)$ and connection overlap. **(B)** Relationship between $max(KS)$ and the correlation between two empirical networks nodal degree. **(C)** Relationship between connection overlap and the correlation between two empirical networks nodal degree. The kernel density plots show the distributions for each parcellation on the respective feature.

On average, topological similarity ($\max(KS)$) between individual empirical and synthetic networks generally occupied a similar range to inter-individual similarity, with over 94% of *matching*, *gene similarity*, and *temporal similarity* GNM networks within the range of interindividual empirical-empirical values (other models showed 6-83% overlap; **Figure 7A**). However, for measures of topography (i.e., connection overlap and degree correlation), empirical-synthetic network comparisons showed almost no overlap with the range of values recorded in empirical-empirical networks (**Figure 7B**). Overall, this result demonstrates that topographic similarity can show wide variation even within a constrained range of $\max(KS)$ values.

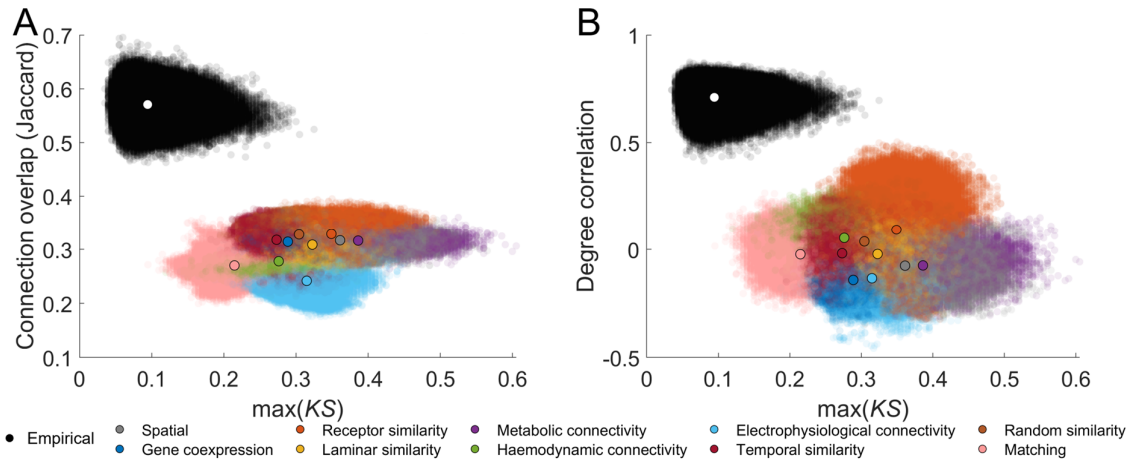

Figure 7. Performance of $\max(KS)$ in empirical networks. Scatter plots depict the relationship between $\max(KS)$ and **(A)** connection overlap; and **(B)** degree correlation for both empirical-synthetic (GNM-produced vs. empirical networks) and empirical-empirical (empirical network vs. empirical network) comparisons. In each plot, the black-outlined dot represents the mean value for each models empirical-synthetic comparisons, with the white dot indicating the mean for empirical-empirical comparisons. The networks with the lowest $\max(KS)$ value for each participant were extracted, and their similarity to all other empirical participant networks was computed. Additionally, all pairs of individual empirical networks were compared using each similarity metric. All empirical networks were generated via probabilistic tractography and using the Schaefer 400 parcellation.

Different similarity measures do not identify more topographically similar networks

Our analysis reveals that the $\max(KS)$ statistic is sensitive to small changes in short-range connectivity (**Figure 5**), but is not sensitive to large differences in long-range connectivity. We next assessed if alternative measures of network similarity could identify networks with greater topologic and topographic similarity to empirical data (**Table S2-S3**). These alternatives were informed by approaches proposed by other studies (Akarca et al., 2022; Goñi et al., 2013; Liu et al., 2024), including TND (similarity across global measures of topology), TF_{diff} (Euclidean norm of the difference between correlation matrices of topological features), $\max(r_d)$ (maximum Pearson distance across degree/clustering/betweenness/connection length), and $\max(RMSE)$ (maximum mean-root-squared error across degree/clustering/closeness/connection length).

We first compared how the different similarity measures performed in the rewiring analysis, finding that the alternative measures showed a rate of change equal to or lower than that of $\max(KS)$ (**Figure S12**). Next, we computed the similarity of each network generated during the optimisation using these alternative measures. While the optimisation procedure was intended to maximise $\max(KS)$, as this procedure densely samples the entire parameter space, it allows for exploration if other parameters can produce a network

similar to the empirical data. For each individual empirical network a) the most similar network (under each metric) generated during the optimisation was selected, and b) the similarity of this network to all other individual empirical networks was taken. As with $\max(KS)$, no alternative metric identified synthetic networks with both a high degree correlation and connection overlap to empirical data (**Figure 8**). Some measures— $\max(r_d)$ and $\max(RMSE)$—indicated that synthetics networks were distinct from empirical networks (Figure **8A, B, E, F**), (TND, TF_{diff}) identified networks that were as similar to empirical networks as empirical networks were to each other (mean overlap across GNMs: $TND = 99\%$; $TF_{diff} = 99\%$; **Figure 8C, D, G, H**). Like with $\max(KS)$, the measures which suggested the generated networks were similar to the empirical data assessed topological properties, while those showing the networks were dissimilar also assessed topography. None of the alternative measures identified networks that were topographically similar to empirical data. Together, these findings indicate that alternative objective functions are unlikely to identify networks produced by GNMs that show greater topographical correspondence with empirical data.

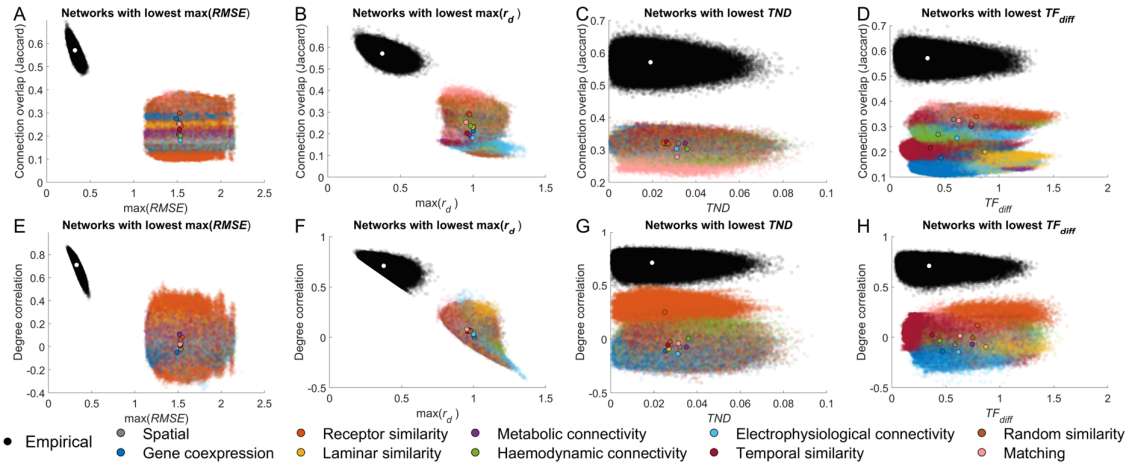

Figure 8. Performance of different similarity measures in generative network models (GNMs) and empirical networks. Scatter plots depict the relationship between connection overlap and **(A)** $\max(RMSE)$; **(B)** $\max(r_d)$; **(C)** TND; and **(D)** TF_{diff} for both empirical-synthetic (GNM-produced vs. empirical networks) and empirical-empirical (empirical network vs. empirical network) comparisons. Similarly, scatter plots show the relationship between degree correlation and **(E)** $\max(RMSE)$; **(F)** $\max(r_d)$; **(G)** TND; and **(H)** TF_{diff} for the same comparisons. In each plot, the black-outlined dot represents the mean value for each models empirical-synthetic comparisons, with the white dot indicating the mean for empirical-empirical comparisons. For each similarity measure, the networks with the lowest value for each participant were extracted, and their similarity to all other empirical participant networks was computed. Additionally, all pairs of individual empirical networks were compared using each similarity metric. All empirical networks were generated via probabilistic tractography and using the Schaefer 400 parcellation.

Discussion

GNMs offer a powerful framework for investigating potential mechanisms and constraints of human brain network organisation. Nonetheless, our results establish that many popular topological GNMs routinely fail to capture critical topographical network organisation due to inaccurate reconstruction of long-range connections between cortical hubs. This is because traditional measures used for model optimization and evaluation based on the similarity of network topology are biased toward the reconstruction of short-range connections. GNMs prioritizing similarity of regional anatomical, cellular, molecular, or dynamical features also fail to overcome this bias, with selection of edges based on similarity in random data showing comparable performance. Our findings therefore indicate that current approaches for defining and fitting GNMs do not identify any single model or parameter combination that can produce a network which accurately captures both the topology and topography of empirical connectome data.

Our analysis indicates that a major reason for the noted failure of extant GNMs to capture connectome topography, particularly the degree sequence of empirical data (Arnatkevičiūtė et al., 2021; Y. Chen et al., 2017; Oldham, Fulcher, et al., 2022; Zhang et al., 2021), is that the models do not reproduce the specific node-node pairing of long-range connections, which play a critical role in shaping the rich-club organisation of the brain (Arnatkevičiūtė et al., 2021; Fulcher & Fornito, 2016; van den Heuvel et al., 2012; van den Heuvel & Sporns, 2011, 2013). This is because these connections to not have a major impact on the $\max(KS)$ statistic, which is the objective function most often used to optimize GNM parameters.

In the GNMs evaluated here, long-range connections impart a significant wiring cost, D_{ij}. A high value of regional or topological similarity, F_{ij}, is therefore required to overcome this distance penalty and increase the probability of connection. In every formulation tested, empirically-connected and unconnected edges could not be clearly distinguished based on a given feature at longer distances (**Figure 4A**), namely because the extent of biological similarity between unconnected regions was similar to or greater than the similarity of connected regions. This observation appears to stand in contrast to previous studies demonstrating that structurally connected cortical areas are on average more

similar to each other than to unconnected areas (Arnatkevičiūtė et al., 2018; Arnatkevičiūtė et al., 2021; Fulcher & Fornito, 2016; Hansen et al., 2023; Hilgetag et al., 2019; Wei et al., 2019), or that hubs regions share similar patterns of gene expression and cortical structure (Arnatkevičiūtė et al., 2021; Paquola et al., 2019, 2020; Sydnor et al., 2021). However recent the extent of biological assortativity may vary with distance in the brain, with short range connections existing being biologically similar regions and long range connections being between biologically dissimilar regions (Bazinet et al., 2023; Betzel & Bassett, 2018; Markov et al., 2013). Currently GNMs cannot model such a distance dependency, which may partially account for why long-range connections cannot be accurately captured.

Compounding the issue of GNMs accurately capturing connectivity is that $\max(KS)$, the primary measure used to determine network similarity, is sensitive to differences in short-range, but not long-range connectivity. Short-range connections most heavily contribute to defining $\max(KS)$, therefore GNMs that can accurately capture the arrangement of short-range connections will perform well on this measure. This accounts for why many models achieve a low $\max(KS)$ as the most probable connections are short-range, even when based on randomly spatially autocorrelated features (**Figure 4C; Figure S8**). This also means that different GNMs can produce very different networks to each other, yet be gauged as equally similar to the empirical data merely because they have accurately captured short-range connections. Conversely, if a network accurately recaptures long-range connectivity, and therefore likely topographical properties, but not short-range connectivity it will do poorly on $\max(KS)$. In either case, it is clear that $\max(KS)$ does not provide a complete picture of the data, thus using it as an objective function on it to identify the most similar network to the modelled data may therefore result in overly optimistic estimates of the extent to which a given model captures desired empirical properties.

The choice of an objective function for GNMs is non-trivial (Betzel & Bassett, 2017). For example if the objective function was defined as connection overlap, this could result in a synthetic network that accurately recaptures many empirical connections but has a radically different topology (Betzel et al., 2016; Betzel & Bassett, 2017). However, our results show that the opposite is also true, two networks can have a very similar topology despite few overlapping edges. Objective functions are selected on the basis they are capturing key relevant properties of the network (Betzel et al., 2016; Betzel & Bassett,

2017). The class of GNMs used in this paper were developed to provide a parsimonious description of the connectomes organisation with respect to its topology, therefore the objective function (i.e., $\max(KS)$) was designed to reflect this (Betzel et al., 2016). It is unlikely that optimising for topology will produce a network with a prescribed topography, as a network with a given topology can have a large number of different topographical representations (Kaiser & Hilgetag, 2006). While important, topology alone cannot explain the entire organisation of the connectome. The spatial embedding of connectivity dictates the function of brain networks (Gollo et al., 2018; Kaiser & Hilgetag, 2006; Pang et al., 2023; Roberts et al., 2016) and is therefore a crucial organisational property. If GNMs are to be used to make stronger claims about the mechanisms and constraints of the organisation of the connectome, amending the objective function to reflect topographical similarity will likely be needed.

Improving generative network models

Our findings indicate that current GNMs offer an insufficient account of both the topology and topography of human connectomes mapped with diffusion MRI. It is useful to reflect on the potential reasons for this failure as a way of improving the biological accuracy of the models.

One possible factor limiting the accuracy of these models is that they fail to account for regional differences in the timing with which different connections form, a phenomenon known as developmental heterochronicity (Beul et al., 2018; Goulas, Betzel, et al., 2019; Goulas, Majka, et al., 2019; Hilgetag et al., 2019). Differential timing of cortical network development has been suggested as a mechanism underlying the emergence of network features like hubs and long-range connections (Kaiser, 2017; Oldham, Ball, et al., 2022; Oldham & Fornito, 2019). Prior work indicates that incorporating global developmental changes in geometry can improve model fits (Oldham, Fulcher, et al., 2022), but imbuing GNMs with regionally patterned windows within which specific connections are formed may be critical for shaping the degree topography of the human brain. Indeed, it has been noted that areas with poorer laminar differentiation complete neurogenesis and start forming connections earlier than areas with more pronounced differentiation (Beul et al., 2017; Cahalane et al., 2012; Epihova et al., 2024; Finlay & Uchiyama, 2015; Scholtens et al., 2014; van den Heuvel et al., 2015). Since network hubs tend to be located in transmodal regions

that show poorer differentiation than primary sensory cortices (Buckner et al., 2009; Margulies et al., 2016), they may obtain an early advantage that drives a rich-get-richer phenomenon known to play a critical role in the emergence of network hubs in a diverse array of systems (Barabási & Albert, 1999; Nicosia et al., 2013).

The best way to parameterize such regional heterochronicity remains unclear. Although cytoarchitectonic similarity has been proposed as a key criterion (Arnatkevičiūtė et al., 2021; Barbas, 2015; Beul et al., 2017, 2018; Hilgetag et al., 2019; Oldham, Fulcher, et al., 2022), as some evidence suggests that dissimilar regions may be more likely to be connected across long distances (Bazinet et al., 2023; Betzel & Bassett, 2018; Markov et al., 2013), models may need to account for a distance-dependent homophilic attachment mechanism. An alternative approach is to move away from models focused on pairwise interactions between regions to capture dynamic properties such as axonal growth (Goulas, Betzel, et al., 2019; Liu et al., 2024; Song et al., 2014). Such models have been implemented for simple 2D or 3D representations of the cortical surface (Goulas, Betzel, et al., 2019; Liu et al., 2024; Song et al., 2014) but could be extended to incorporate the complex geometry of the human brain. These more biophysical models would also have the advantage of easily allowing for connection weights to be modelled, and potentially allow for the shape of the formed tracts to be examined (Liu et al., 2024), providing additional angles with which to evaluate the synthetically produced connectivity.

Limitations

Diffusion MRI is plagued by various biases that can limit the biological veracity of empirical connectome data. Although multiple approaches have been developed to mitigate some of these biases (Baum et al., 2018; Oldham et al., 2020) variations between these methods can yield networks with major differences in topology and topography (Gajwani et al., 2023; Oldham et al., 2020). It is therefore possible that GNMs applied to data processed using one pipeline may not generalize to data processed in other ways. However, GNMs have been performed on primate structural brain networks created using tract tracing data and achieve similar performance to what is obtained in human brain networks (Y. Chen et al., 2017), implying that the issues we have identified in GNMs are not merely a result of using human tractography data.

We did not consider the weighted topology/topography of empirical connectomes, which is a salient feature of brain networks (Fornito et al., 2016; Markov et al., 2011). One recent GNM has been proposed to model connection weights, and shown promise in capturing binary and weighted features (Akarca et al., 2023), although it remains to be seen if the reported model fits, which rely on a similar approach to that investigated here, are subject to the same biases. Our models were restricted to just a single hemisphere of the cortex for computational tractability, and because long-range inter-hemispheric connections are reconstructed with limited accuracy using diffusion MRI. Expanding GNMs to capture these connections, as well as the complex connectivity patterns linking cortex and subcortex (Müller et al., 2020; Oldham & Ball, 2023; Park et al., 2024; Raut et al., 2020; Tian et al., 2020), is needed to achieve a more comprehensive understanding of mechanisms underpinning all connectome organisation.

Conclusion

GNMs can successfully replicate basic topological properties of brain networks but they fall short in capturing topographical properties, particularly the crucial long-range connections observed in empirical data. Additionally, the common practice of evaluating model fits purely based on topology may overlook the true extent of differences between networks. Our findings establish where and why generative network models struggle in capturing brain connectivity and indicate directions for future research to address these challenges and improve model accuracy.

Methods

Empirical brain networks

Two empirical datasets were used in this study, a group averaged connectivity matrix (Hansen et al., 2023) and a set of individualised connectivity matrices (Arnatkevičiūtė et al., 2021; Oldham, Fulcher, et al., 2022). Both datasets were constructed from Human Connectome Project (HCP) data. The group averaged data had been constructed from the S900 release of the HCP data from 326 participants. In brief, the preprocessed diffusion data had been processed with MRtrix3 using multi-shell multi-tissue constrained spherical deconvolution and tractography was conducted with second-order Integration over Fiber

Orientation Distributions (iFOD2). Streamlines were weighted using SIFT2 (Smith et al., 2015), and the group consensus connectivity matrix was created using a distance dependant thresholding algorithm. Further details are available in Hasnen et al., (2023). The group connectivity matrix was binarized for use in this study. The dataset was originally created for the full Schaefer 400, 7 network parcellation (Schaefer et al., 2018), which includes 200 regions for each hemisphere. We only used data for the left hemisphere i.e., 200 cortical regions in total as to: a) reduce computational complexity (more nodes/connections in the network increases the time needed to run the GNM) b) reduce any bias that may result of measuring the Euclidean distance from nodes across hemispheres, and c) keep consistent with previous methodologies (Arnatkevičiūtė et al., 2021; Betzel et al., 2016; Oldham, Fulcher, et al., 2022).

The individualised connectivity data had also previously been processed (Arnatkevičiūtė et al., 2021; Oldham, Fulcher, et al., 2022). These data were constructed from the S1200 release of the HCP for 973 participants. A similar series of processing steps were applied as with first dataset. In addition to iFOD2, a probabilistic tractography algorithm, the deterministic algorithm Fiber Assignment by Continuous Tractography was also run. Further details of the processing steps for the individualised data are available elsewhere (Arnatkevičiūtė et al., 2021; Oldham, Fulcher, et al., 2022). We generated a network for each of the Schaefer 7 network 100-1000 parcellations, using the probabilistic and deterministic tractograms resulting in 20 networks per participant (two different tractograms across 10 different parcellations). As with the group averaged data, we only retained regions in the left hemisphere. One of the networks of the 973 showed noticeably altered connectivity compared to others (i.e., lower density, weaker correlations with other individuals), thus they were excluded from further analysis.

Networks were either unthresholded or thresholded based on connection strength. Thresholding was applied such that only the strongest *E* connections were retained, where *E* was 70% of the minimum density observed for any individual in a given tractography/parcellation combination. While a strength threshold is likely to result in weak, long-range connections being pruned, we used this approach as to ensure that all individuals for a given network type had the same density with some variation in their topology. Other thresholding approaches involve the creation of a consensus matrix which is

then used as a mask for individuals (Betzel et al., 2019; de Reus & van den Heuvel, 2013; Roberts et al., 2017), but such approaches would minimize inter-individual variability in network binary network topology and thus meaning there would be little value in comparing individual binary network organisation.

Cortical interregional similarity measures

We used seven different measures of interregional similarity which represent multiple facets of brain organisation (Hansen et al., 2023): (1) gene co-expression (correlation across 8687 genes); (2) receptor similarity (correlation across 18 PET receptor density profiles); (3) laminar similarity (correlation across cortical layer histology); (4) metabolic coupling (correlation in PET timeseries); (5) haemodynamic coupling (correlation in fMRI timeseries); (6) electrophysiological coupling (correlation in MEG timeseries); and (7) temporal similarity (correlation across 6441 fMRI timeseries features). These measures had previously been generated for the Schaefer 400 parcellation and made openly available as part of another study (see Hansen et al., 2023 for details). All measures of interregional similarity were provided as a matrix of Pearson correlations. For use with GNMs, each correlation matrix was converted to a Pearson distance (as GNMs cannot tolerate negative values for interregional similarity) and then rescaled to the unit interval.

These regional measures are representative of major organisational patterns in the cortex (Hansen et al., 2023; Markello et al., 2022). However these regional measures can demonstrate spatial autocorrelations which can explain many properties of the brain (Burt et al., 2020; Markello & Misic, 2021; Shinn et al., 2023). To assess the impact of spatial autocorrelations in GNMs, we created random spatially autocorrelated features and computed regional similarity on those using the following procedure:

1. We generated a random value in the range 0-1 for each cortical region.
2. For each cortical region, we took the average value of each of the nodes it was adjacent to on the cortical surface.
3. We then updated the value of each cortical region to this averaged value (note this was only done once all the averaged values for all regions had been calculated).
4. Steps 2-3 were repeated a further four times.

5. Steps 1-4 were repeated 20 times to create 20 random spatially autocorrelated features.
6. Random interregional similarity was calculated by performing a Pearson correlation across each of these random features for every pair of brain regions.

While there are more sophisticated approaches of creating spatially autocorrelated cortical features (Burt et al., 2020), this approach is a fast and efficient way of creating multiple such maps. As with the other measures of interregional similarity, the Pearson correlation was converted to a Pearson distance and then rescaled to the unit interval. In addition to these measures of interregional similarity, we also examined 12 topological based models (**Table S1**).

Additionally Euclidean distances between all pairs of nodes were calculated to get an estimate of wiring-costs for the GNM. Specifically, the Euclidean distance was taken as the average distance from all the vertices on the cortical surface that were assigned to one region, to all the vertices assigned to another region. Euclidean distances do not account for the curved paths tracts have to take i.e., fibre distances, and so can underestimate the true wiring costs. While more elaborate procedures exist for approximating the fibre lengths and therefore wiring-costs (Oldham, Fulcher, et al., 2022), Euclidean and fibre distances are often strongly correlated (Betzel et al., 2016), and using either to predict connections in brain networks has resulted in similar performance (Rubinov et al., 2015). We therefore deemed Euclidean distances as an acceptable approximation of wiring-costs for within hemisphere connectivity.

Generative network model formulation

The generative network model adds connections in a sequential manner up to the desired number (i.e., the number of connections in the network the model is attempting to replicate) according to the wiring rule

$$w_{ij} = f(\mathrm{e}^{-\eta D_{ij}}) + \alpha f\left({F_{ij}}^{\gamma}\right). \tag{2}$$

As indicated by Equation 2, GNMs were primarily formulated as an additive rule, and the distance decay was defined according to an exponential. This additive rule has previously been shown to more accurately capture the trade-offs between model

parameters implied by the model than alternative, multiplicative formulations (Oldham, Fulcher, et al., 2022). Alternative the rule could be formulated as a multiplication of terms

$$w_{ij} = f(\mathrm{e}^{-\eta D_{ij}}) \times f\left({F_{ij}}^{\gamma}\right). \tag{3}$$

While we primarily model distance as an exponential decay $\mathrm{e}^{-\eta D_{ij}}$ due to evidence showing the likelihood of a connection existing decreases exponential as a function of its length, other studies have used a power-law decay ${D_{ij}}^{-\eta}$ (Betzel et al., 2016) but the specific form of the distance penalty does not change the basic conclusions of our findings. The term F_{ij} can either represent some measure of similarity on a cortical measure, like gene expression or haemodynamics (**Table 1**), or indicate some form of topological coupling (**Table S1**).

At each timestep of the model, each scaled term S_{ij} i.e., $\mathrm{e}^{-\eta D_{ij}}$, ${D_{ij}}^{-\eta}$ or ${F_{ij}}^{\gamma}$ is normalised according to

$$f\left(S_{ij}\right) = \frac{S_{ij}}{\max\left(\left\{S_{ij} \middle| A_{uv} = 0\right\}\right)}, \tag{4}$$

which normalises the scaled distance/feature according to the maximum scaled value. At each timestep of the model, each normalised term and hence w_{ij} is recalculated due to the normalisation being performed based on connections that are not present in the network, which changes at each timestep.

The weight w_{ij} is converted to a probability at each timestep of the GNM

$$P_{ij} = \frac{w_{ij}(1 - A_{ij})}{\sum_u \sum_{v>u} w_{uv}(1 - A_{uv})}, \tag{5}$$

where the $(1 - A_{ij})$ ensures that only connections that are not yet present in the network influence the connection probability (i.e., the probability of a connection forming should only be relative to other connections that have not formed yet). At each timestep a single connection is established, with P_{ij} indicating the probability that specific connection will be selected. If F_{ij} is a measure of topology, that measure will be recalculated based on the network will the newly added connection.

As w_{ij} will change at each timestep of the model, so will P_{ij}. Therefore, to calculate the overall probability a given connection will form, we average connections probabilities across model timestep (note the average was only calculated for iterations where the connection had not been added into the network).

Selecting optimised generative network models

To determine the optimal values for the parameters η, γ, and α for each GNM, we employed a previously developed optimization method (Betzel et al., 2016; Oldham, Fulcher, et al., 2022). The method was implemented as follows:

1. We randomly sampled 2000 points within the parameter space defined by η, γ, and potentially α (if the additive form was used). When an exponential was used, η varied between 0 and 2, and varied between 0 and 10 when a power-law with a power-law. For GNMs that used interregional similarity, γ varied between -20 and 200 but with topology it varied between -10 and 10, and α ranged between 0 and 10 (when α was included as a parameter in the model; parameter ranges had been selected based on initial testing).
2. At each sampled point representing a specific combination of η, γ, and α values, we generated a network using the newly defined parameters, resulting in 2000 synthetic networks. We calculated the $\max(KS)$ statistic for each generated network. The $\max(KS)$ statistic is the maximum KS value (i.e., greatest discrepancy) between the generated and empirical networks in terms of their degree, clustering, betweenness centrality, and connection length distributions.
3. After evaluating all networks, we employed Voronoi tessellation to identify regions (cells) of the parameter space associated with low fit statistics. An additional 2000 points in the parameter space were preferentially sampled from each cell based on the relative probability $VC_c^{-\beta}$, where VC_c is the $\max(KS)$ of cell c, and β controls the likelihood of sampling from cells with low $\max(KS)$ values.
4. Steps 2 and 3 were repeated four times, resulting in a total of 10,000 points being evaluated. In each repetition, the probability of sampling cells with better fits was increased by varying β from 0.5 to 2 in 0.5 increments, thus converging to an approximate optimum. When the optimisation was applied to the ensemble of

individual networks, the network generated by the model for a given parameter combination was compared to all individual networks (Liu et al., 2023). The $\max(KS)$ for that parameter combination was taken as the mean of all individual $\max(KS)$ values. The networks generated during the optimisation that produced the lowest $\max(KS)$ for an individual participant were used for subsequent analyses. When evaluating other similarity measures, we used the networks generated when optimising for $\max(KS)$ because (1) there was a greater computational cost to running the GNM again with a different fit statistics and (2), the parameter space is densely sampled so examining from the networks selected is likely to allow the identification of a minimum.

An advantage of this approach is that it allows for the entire parameter space to be adequately sampled and facilitate the identification of a global (approximate) optimum. For the group-averaged consensus network, when the optimal parameters had been identified for a given GNM they were used to generate 100 further networks.

Rewiring model

Networks were rewired at random, or from the shortest-to-longest connections, or longest-to-shortest. Existing connections could only be rewired/swapped with a non-exiting connection. Once a connection had been rewired, it could not be rewired again. Connections could be rewired with a selected non-existing connection at random, a connection of a similar length, or a connection of dissimilar length. The rewiring continued until all existing connections had been rewired. We ran each rewiring model 30 times and then took the mean $\max(KS)$ across these runs.

Measures of network topology/topography

Details of the various topological/topographical measures used in this study can be found in Tables S1, S2, and S3.

Code and data availability

All analysis was performed in MATLAB 2023b. Code and data are available from https://github.com/StuartJO/ComingUpShort

Acknowledgements

Data were provided by the Human Connectome Project, WU-Minn Consortium (Principal Investigators: David Van Essen and Kamil Ugurbil; 1U54MH091657) funded by the 16 NIH Institutes and Centers that support the NIH Blueprint for Neuroscience Research and by the McDonnell Center for Systems Neuroscience at Washington University. S.O is supported by the Brain and Behavior Research Foundation (ID: 31471). A.F. was supported by the Sylvia and Charles Viertel Foundation, National Health and Medical Research Council (IDs: 1197431 and 1146292), and Australian Research Council (IDs: DP200103509). G.B. was support by the National Health and Medical Research Council (ID: 1194497). This research was supported by the Murdoch Children's Research Institute, the Royal Children's Hospital, Department of Paediatrics, The University of Melbourne and the Victorian Government's Operational Infrastructure Support Program. The project was generously supported by The Royal Children's Hospital Foundation devoted to raising funds for research at The Royal Children's Hospital.

References

Akarca, D., Dunn, A. W. E., Hornauer, P. J., Ronchi, S., Fiscella, M., Wang, C., Terrigno, M., Jagasia, R., Vértes, P. E., Mierau, S. B., Paulsen, O., Eglen, S. J., Hierlemann, A., Astle, D. E., & Schröter, M. (2022). *Homophilic wiring principles underpin neuronal network topology* in vitro. https://doi.org/10.1101/2022.03.09.483605

Akarca, D., Schiavi, S., Achterberg, J., Genc, S., Jones, D. K., & Astle, D. E. (2023). A weighted generative model of the human connectome. *bioRxiv*, 2023.06.23.546237. https://doi.org/10.1101/2023.06.23.546237

Akarca, D., Vértes, P. E., Bullmore, E. T., CALM team, & Astle, D. E. (2021). A generative network model of neurodevelopmental diversity in structural brain organization. *Nature Communications*, *12*(1), 4216. https://doi.org/10.1038/s41467-021-24430-z

Albert, R., & Barabási, A. L. (2002). Statistical mechanics of complex networks. *Reviews of Modern Physics*, *74*(1), 47–97. https://doi.org/10.1103/RevModPhys.74.47

Arnatkevičiūtė, A., Fulcher, B. D., Oldham, S., Tiego, J., Paquola, C., Gerring, Z., Aquino, K., Hawi, Z., Johnson, B., Ball, G., Klein, M., Deco, G., Franke, B., Bellgrove, M. A., & Fornito, A. (2021). Genetic influences on hub connectivity of the human connectome. *Nature Communications*, *12*(1), 4237. https://doi.org/10.1038/s41467-021-24306-2

Arnatkevičiūtė, A., Fulcher, B. D., Pocock, R., & Fornito, A. (2018). Hub connectivity, neuronal diversity, and gene expression in the Caenorhabditis elegans connectome. *PLoS Computational Biology*, *14*(2), 1–32. https://doi.org/10.1371/journal.pcbi.1005989

Barabási, A.-L., & Albert, R. (1999). Emergence of Scaling in Random Networks. *Science*, *286*(October), 509–512. https://doi.org/10.1126/science.286.5439.509

Barbas, H. (1986). Pattern in the laminar origin of corticocortical connections. *Journal of Comparative Neurology*, *252*(3), 415–422. https://doi.org/10.1002/cne.902520310

Barbas, H. (2015). General Cortical and Special Prefrontal Connections: Principles from Structure to Function. *Annual Review of Neuroscience*, *38*, 269–289. https://doi.org/10.1146/annurev-neuro-071714-033936

Bassett, D. S., & Bullmore, E. T. (2006). Small-World Brain Networks. *The Neuroscientist*, *12*(6), 512–523. https://doi.org/10.1177/1073858406293182

Bassett, D. S., & Bullmore, E. T. (2017). Small-World Brain Networks Revisited. *Neuroscientist*, *23*(5), 499–516. https://doi.org/10.1177/1073858416667720

Bassett, D. S., Bullmore, E. T., Verchinski, B. a, Mattay, V. S., Weinberger, D. R., & Meyer-Lindenberg, A. (2008). Hierarchical Organization of Human Cortical Networks in Health and Schizophrenia. *Journal of Neuroscience*, *28*(37), 9239–9248. https://doi.org/10.1523/JNEUROSCI.1929-08.2008

Baum, G. L., Roalf, D. R., Cook, P. A., Ciric, R., Rosen, A. F. G., Xia, C., Elliott, M. A., Ruparel, K., Verma, R., Tunç, B., Gur, R. C., Gur, R. E., Bassett, D. S., & Satterthwaite, T. D. (2018). The impact of in-scanner head motion on structural connectivity derived from diffusion MRI. *NeuroImage*, *173*, 275–286. https://doi.org/10.1016/j.neuroimage.2018.02.041

Bazinet, V., Hansen, J. Y., Vos De Wael, R., Bernhardt, B. C., Van Den Heuvel, M. P., & Misic, B. (2023). Assortative mixing in micro-architecturally annotated brain connectomes. *Nature Communications*, *14*(1), 2850. https://doi.org/10.1038/s41467-023-38585-4

Betzel, R. F., Avena-Koenigsberger, A., Goñi, J., He, Y., de Reus, M. A., Griffa, A., Vértes, P. E., Mišić, B., Thiran, J. P., Hagmann, P., van den Heuvel, M. P., Zuo, X. N., Bullmore, E. T., & Sporns, O. (2016). Generative models of the human connectome. *NeuroImage*, *124*, 1054–1064. https://doi.org/10.1016/j.neuroimage.2015.09.041

Betzel, R. F., & Bassett, D. S. (2017). Generative models for network neuroscience: Prospects and promise. *Journal of The Royal Society Interface*, *14*(136), 20170623. https://doi.org/10.1098/rsif.2017.0623

Betzel, R. F., & Bassett, D. S. (2018). Specificity and robustness of long-distance connections in weighted, interareal connectomes. *Proceedings of the National Academy of Sciences*, *115*(21), E4880–E4889. https://doi.org/10.1073/pnas.1720186115

Betzel, R. F., Griffa, A., Hagmann, P., & Mišić, B. (2019). Distance-dependent consensus thresholds for generating group-representative structural brain networks. *Network Neuroscience*, *3*(2), 475–496. https://doi.org/10.1162/netn_a_00075

Beul, S. F., Barbas, H., & Hilgetag, C. C. (2017). A Predictive Structural Model of the Primate Connectome. *Scientific Reports*, *7*, 43176. https://doi.org/10.1038/srep43176

Beul, S. F., Goulas, A., & Hilgetag, C. C. (2018). Comprehensive computational modelling of the development of mammalian cortical connectivity underlying an architectonic type principle. *PLoS Computational Biology*, *14*(11), 1–45. https://doi.org/10.1371/journal.pcbi.1006550

Buckner, R. L., Sepulcre, J., Talukdar, T., Krienen, F. M., Liu, H., Hedden, T., Andrews-Hanna, J. R., Sperling, R. A., & Johnson, K. A. (2009). Cortical hubs revealed by intrinsic functional connectivity: Mapping, assessment of stability, and relation to Alzheimer's disease. *Journal of Neuroscience*, *29*(6), 1860–1873. https://doi.org/10.1523/JNEUROSCI.5062-08.2009

Bullmore, E. T., & Sporns, O. (2009). Complex brain networks: Graph theoretical analysis of structural and functional systems. *Nature Reviews Neuroscience*, *10*(3), 186–198. https://doi.org/10.1038/nrn2575

Bullmore, E. T., & Sporns, O. (2012). The economy of brain network organization. *Nature Reviews Neuroscience*, *13*(5), 336–349. https://doi.org/10.1038/nrn3214

Burt, J. B., Helmer, M., Shinn, M., Anticevic, A., & Murray, J. D. (2020). Generative modeling of brain maps with spatial autocorrelation. *NeuroImage*, *220*, 117038. https://doi.org/10.1016/j.neuroimage.2020.117038

Cahalane, D. J., Charvet, C. J., & Finlay, B. L. (2012). Systematic, balancing gradients in neuron density and number across the primate isocortex. *Frontiers in Neuroanatomy*, *6*, 12. https://doi.org/10.3389/fnana.2012.00028

Carozza, S., Akarca, D., & Astle, D. (2023). The adaptive stochasticity hypothesis: Modeling equifinality, multifinality, and adaptation to adversity. *Proceedings of the National Academy of Sciences*, *120*(42), e2307508120. https://doi.org/10.1073/pnas.2307508120

Chen, B. L., Hall, D. H., & Chklovskii, D. B. (2006). Wiring optimization can relate neuronal structure and function. *Proceedings of the National Academy of Sciences*, *103*(12), 4723–4728. https://doi.org/10.1073/pnas.0506806103

Chen, Y., Wang, S., Hilgetag, C. C., & Zhou, C. (2013). Trade-off between Multiple Constraints Enables Simultaneous Formation of Modules and Hubs in Neural Systems. *PLoS Computational Biology*, *9*(3), 31–33. https://doi.org/10.1371/journal.pcbi.1002937

Chen, Y., Wang, S., Hilgetag, C. C., & Zhou, C. (2017). Features of spatial and functional segregation and integration of the primate connectome revealed by trade-off between wiring cost and efficiency. *PLOS Computational Biology*, *13*(9), e1005776. https://doi.org/10.1371/journal.pcbi.1005776

Cherniak, C., Mokhtarzada, Z., Rodriguez-Esteban, R., & Changizi, K. (2004). Global optimization of cerebral cortex layout. *Proceedings of the National Academy of Sciences*, *101*(4), 1081–1086. https://doi.org/10.1073/pnas.0305212101

Chklovskii, D. B. (2004). Synaptic connectivity and neuronal morphology: Two sides of the same coin. *Neuron*, *43*(5), 609–617.

Chklovskii, D. B., Schikorski, T., & Stevens, C. F. (2002). Wiring optimization in cortical circuits. *Neuron*, *34*(3), 341–347. https://doi.org/10.1016/S0896-6273(02)00679-7

de Reus, M. a., & van den Heuvel, M. P. (2013). Estimating false positives and negatives in brain networks. *NeuroImage*, *70*, 402–409. https://doi.org/10.1016/j.neuroimage.2012.12.066

Deco, G., Sanz Perl, Y., Vuust, P., Tagliazucchi, E., Kennedy, H., & Kringelbach, M. L. (2021). Rare long-range cortical connections enhance human information processing. *Current Biology*, *31*(20), 4436-4448.e5. https://doi.org/10.1016/j.cub.2021.07.064

Epihova, G., Epihov, D. Z., Akarca, D., & Astle, D. E. (2024). *Molecular mechanisms driving divergent development of the human frontal and visual cortex during prenatal development*. https://doi.org/10.1101/2024.05.15.594422

Ercsey-Ravasz, M., Markov, N. T., Lamy, C., Van Essen, D. C., Knoblauch, K., Toroczkai, Z., Kennedy, H., VanEssen, D. C., Knoblauch, K., Toroczkai, Z., & Kennedy, H. (2013). A Predictive Network Model of Cerebral Cortical Connectivity Based on a Distance Rule. *Neuron*, *80*(1), 184–197. https://doi.org/10.1016/j.neuron.2013.07.036

Finlay, B. L., & Uchiyama, R. (2015). Developmental mechanisms channeling cortical evolution. *Trends in Neurosciences*, *38*(2), 69–76. https://doi.org/10.1016/j.tins.2014.11.004

Fornito, A., Arnatkevičiūtė, A., & Fulcher, B. D. (2019). Bridging the Gap between Connectome and Transcriptome. *Trends in Cognitive Sciences*, *23*(1), 34–50. https://doi.org/10.1016/j.tics.2018.10.005

Fornito, A., Zalesky, A., & Bullmore, E. T. (2016). *Fundamentals of Brain Network Analysis*. Academic Press.

Fulcher, B. D., & Fornito, A. (2016). A transcriptional signature of hub connectivity in the mouse connectome. *Proceedings of the National Academy of Sciences*, *113*(5), 1435–1440. https://doi.org/10.1073/pnas.1513302113

Gajwani, M., Oldham, S., Pang, J. C., Arnatkevi, A., Tiego, J., Bellgrove, M. A., & Fornito, A. (2023). Can hubs of the human connectome be identified consistently with diffusion MRI? *Network Neuroscience*, *7*(4).

Gollo, L. L., Roberts, J. A., Cropley, V. L., Di Biase, M. A., Pantelis, C., Zalesky, A., & Breakspear, M. (2018). Fragility and volatility of structural hubs in the human connectome. *Nature Neuroscience*, *21*(8), 1107–1116. https://doi.org/10.1038/s41593-018-0188-z

Goñi, J., Avena-Koenigsberger, A., Velez de Mendizabal, N., van den Heuvel, M. P., Betzel, R. F., & Sporns, O. (2013). Exploring the Morphospace of Communication Efficiency in Complex Networks. *PLoS ONE*, *8*(3), e58070. https://doi.org/10.1371/journal.pone.0058070

Goulas, A., Betzel, R. F., & Hilgetag, C. C. (2019). Spatiotemporal ontogeny of brain wiring. *Science Advances*, *5*(6). https://doi.org/10.1126/sciadv.aav9694

Goulas, A., Majka, P., Rosa, M. G. P., & Hilgetag, C. C. (2019). A blueprint of mammalian cortical connectomes. *PLOS Biology*, *17*(3), e2005346. https://doi.org/10.1371/journal.pbio.2005346

Hansen, J. Y., Shafiei, G., Voigt, K., Liang, E. X., Cox, S. M. L., Leyton, M., Jamadar, S. D., & Misic, B. (2023). Integrating multimodal and multiscale connectivity blueprints of the human cerebral cortex in health and disease. *PLOS Biology*, *21*(9), e3002314. https://doi.org/10.1371/journal.pbio.3002314

Henderson, J. A., & Robinson, P. A. (2013). Using Geometry to Uncover Relationships Between Isotropy, Homogeneity, and Modularity in Cortical Connectivity. *Brain Connectivity*, *3*(4), 423–437. https://doi.org/10.1089/brain.2013.0151

Henderson, J. A., & Robinson, P. A. (2014). Relations Between the Geometry of Cortical Gyrification and White-Matter Network Architecture. *Brain Connectivity*, *4*(2), 112–130. https://doi.org/10.1089/brain.2013.0183

Hilgetag, C. C., Beul, S. F., van Albada, S. J., & Goulas, A. (2019). An architectonic type principle integrates macroscopic cortico-cortical connections with intrinsic cortical circuits of the primate brain. *Network Neuroscience*, *3*(4), 905–923. https://doi.org/10.1162/netn_a_00100

Horvát, S., Gămănuț, R., Ercsey-Ravasz, M., Magrou, L., Gămănuț, B., Van Essen, D. C., Burkhalter, A., Knoblauch, K., Toroczkai, Z., & Kennedy, H. (2016). Spatial Embedding and Wiring Cost Constrain the Functional Layout of the Cortical Network of Rodents and Primates. *PLOS Biology*, *14*(7), e1002512. https://doi.org/10.1371/journal.pbio.1002512

Kaiser, M. (2017). Mechanisms of Connectome Development. *Trends in Cognitive Sciences*, *21*(9), 703–717. https://doi.org/10.1016/j.tics.2017.05.010

Kaiser, M., & Hilgetag, C. C. (2004). Modelling the development of cortical systems networks. *Neurocomputing*, *58–60*, 297–302. https://doi.org/10.1016/j.neucom.2004.01.059

Kaiser, M., & Hilgetag, C. C. (2006). Nonoptimal component placement, but short processing paths, due to long-distance projections in neural systems. *PLoS Computational Biology*, *2*(7), 0805–0815. https://doi.org/10.1371/journal.pcbi.0020095

Liu, Y., Seguin, C., Betzel, R. F., Akarca, D., Di Biase, M. A., & Zalesky, A. (2024). *A generative model of the connectome with dynamic axon growth*. https://doi.org/10.1101/2024.02.23.581824

Liu, Y., Seguin, C., Mansour, S., Oldham, S., Betzel, R., Di Biase, M. A., & Zalesky, A. (2023). Parameter estimation for connectome generative models: Accuracy, reliability, and a fast parameter fitting method. *NeuroImage*, *270*, 119962. https://doi.org/10.1016/j.neuroimage.2023.119962

Margulies, D. S., Ghosh, S. S., Goulas, A., Falkiewicz, M., Huntenburg, J. M., Langs, G., Bezgin, G., Eickhoff, S. B., Castellanos, F. X., Petrides, M., Jefferies, E., & Smallwood, J. (2016). Situating the default-mode network along a principal gradient of macroscale cortical organization. *Proceedings of the National Academy of Sciences of the United States of America*, *113*(44), 12574–12579. https://doi.org/10.1073/pnas.1608282113

Markello, R. D., Hansen, J. Y., Liu, Z.-Q., Bazinet, V., Shafiei, G., Suárez, L. E., Blostein, N., Seidlitz, J., Baillet, S., Satterthwaite, T. D., Chakravarty, M. M., Raznahan, A., & Misic, B. (2022). neuromaps: Structural and functional interpretation of brain maps. *Nature Methods*, *19*(11), 1472–1479. https://doi.org/10.1038/s41592-022-01625-w

Markello, R. D., & Misic, B. (2021). Comparing spatial null models for brain maps. *NeuroImage*, *236*, 118052. https://doi.org/10.1016/j.neuroimage.2021.118052

Markov, N. T., Ercsey-Ravasz, M., Lamy, C., Ribeiro Gomes, A. R., Magrou, L., Misery, P., Giroud, P., Barone, P., Dehay, C., Toroczkai, Z., Knoblauch, K., Van Essen, D. C., & Kennedy, H. (2013). The role of long-range connections on the specificity of the macaque interareal cortical network. *Proceedings of the National Academy of Sciences*, *110*(13), 5187–5192. https://doi.org/10.1073/pnas.1218972110

Markov, N. T., Misery, P., Falchier, A., Lamy, C., Vezoli, J., Quilodran, R., Gariel, M. A., Giroud, P., Ercsey-Ravasz, M., Pilaz, L. J., Huissoud, C., Barone, P., Dehay, C., Toroczkai, Z., Van Essen, D. C., Kennedy, H., & Knoblauch, K. (2011). Weight consistency specifies regularities of macaque cortical networks. *Cerebral Cortex*, *21*(6), 1254–1272. https://doi.org/10.1093/cercor/bhq201

Meunier, D., Lambiotte, R., Fornito, A., Ersche, K. D., & Bullmore, E. T. (2009). Hierarchical modularity in human brain functional networks. *Frontiers in Neuroinformatics*, *3*, 37. https://doi.org/10.3389/neuro.11.037.2009

Müller, E. J., Munn, B., Hearne, L. J., Smith, J. B., Fulcher, B., Arnatkevičiūtė, A., Lurie, D. J., Cocchi, L., & Shine, J. M. (2020). Core and matrix thalamic sub-populations relate to spatio-temporal cortical connectivity gradients. *NeuroImage*, *222*, 117224. https://doi.org/10.1016/j.neuroimage.2020.117224

Nicosia, V., Vértes, P. E., Schafer, W. R., Latora, V., & Bullmore, E. T. (2013). Phase transition in the economically modeled growth of a cellular nervous system. *Proceedings of the National Academy of Sciences*, *110*(19), 7880–7885. https://doi.org/10.1073/pnas.1300753110

Oldham, S., Arnatkevičiūtė, A., Smith, R. E., Tiego, J., Bellgrove, M. A., & Fornito, A. (2020). The efficacy of different preprocessing steps in reducing motion-related confounds in diffusion MRI connectomics. *NeuroImage*, *222*, 117252. https://doi.org/10.1016/j.neuroimage.2020.117252

Oldham, S., & Ball, G. (2023). A phylogenetically-conserved axis of thalamocortical connectivity in the human brain. *Nature Communications*, *14*(1), 6032. https://doi.org/10.1038/s41467-023-41722-8

Oldham, S., Ball, G., & Fornito, A. (2022). Early and late development of hub connectivity in the human brain. *Current Opinion in Psychology*, *44*, 321–329. https://doi.org/10.1016/j.copsyc.2021.10.010

Oldham, S., & Fornito, A. (2019). The development of brain network hubs. *Developmental Cognitive Neuroscience*, *36*, 100607. https://doi.org/10.1016/j.dcn.2018.12.005

Oldham, S., Fulcher, B. D., Aquino, K., Arnatkevičiūtė, A., Paquola, C., Shishegar, R., & Fornito, A. (2022). Modeling spatial, developmental, physiological, and topological constraints on human brain connectivity. *Science Advances*, *8*(22), eabm6127. https://doi.org/10.1126/sciadv.abm6127

Pang, J. C., Aquino, K. M., Oldehinkel, M., Robinson, P. A., Fulcher, B. D., Breakspear, M., & Fornito, A. (2023). Geometric constraints on human brain function. *Nature*, *618*(7965), 566–574. https://doi.org/10.1038/s41586-023-06098-1

Paquola, C., Seidlitz, J., Benkarim, O., Royer, J., Klimes, P., Bethlehem, R. A. I., Larivière, S., de Wael, R. V., Rodríguez-Cruces, R., Hall, J. A., Frauscher, B., Smallwood, J., & Bernhardt, B. C. (2020). A multi-scale cortical wiring space links cellular architecture and functional dynamics in the human brain. *PLOS Biology*, *18*(11). https://doi.org/10.1371/journal.pbio.3000979

Paquola, C., Vos De Wael, R., Wagstyl, K., Bethlehem, R. A. I., Hong, S. J., Seidlitz, J., Bullmore, E. T., Evans, A. C., Misic, B., Margulies, D. S., Smallwood, J., & Bernhardt, B. C. (2019).

Microstructural and Functional Gradients are Increasingly Dissociated in Transmodal Cortices. *PLOS Biology*, *17*(5), e3000284. https://doi.org/10.1371/journal.pbio.3000284

Park, S., Haak, K. V., Oldham, S., Cho, H., Byeon, K., Park, B., Thomson, P., Chen, H., Gao, W., Xu, T., Valk, S., Milham, M. P., Bernhardt, B., Martino, A. D., & Hong, S.-J. (2024). *A shifting role of thalamocortical connectivity in the emergence of large-scale functional brain organization during early lifespan*. bioRxiv. https://doi.org/10.1101/2024.03.11.584415

Raichle, M. E., & Mintun, M. A. (2006). Brain work and brain imaging. *Annual Review of Neuroscience*, *29*, 449–476. https://doi.org/10.1146/annurev.neuro.29.051605.112819

Raut, R. V., Snyder, A. Z., & Raichle, M. E. (2020). Hierarchical dynamics as a macroscopic organizing principle of the human brain. *Proceedings of the National Academy of Sciences*, *117*(34), 20890–20897. https://doi.org/10.1073/pnas.2003383117

Rivera-Alba, M., Peng, H., De Polavieja, G. G., & Chklovskii, D. B. (2014). Wiring economy can account for cell body placement across species and brain areas. *Current Biology*, *24*(3), R109–R110. https://doi.org/10.1016/j.cub.2013.12.012

Rivera-Alba, M., Vitaladevuni, S. N., Mischenko, Y., Lu, Z., Takemura, S. Y., Scheffer, L., Meinertzhagen, I. A., Chklovskii, D. B., & De Polavieja, G. G. (2011). Wiring economy and volume exclusion determine neuronal placement in the Drosophila brain. *Current Biology*, *21*(23), 2000–2005. https://doi.org/10.1016/j.cub.2011.10.022

Roberts, J. A., Perry, A., Lord, A. R., Roberts, G., Mitchell, P. B., Smith, R. E., Calamante, F., & Breakspear, M. (2016). The contribution of geometry to the human connectome. *NeuroImage*, *124*, 379–393. https://doi.org/10.1016/j.neuroimage.2015.09.009

Roberts, J. A., Perry, A., Roberts, G., Mitchell, P. B., & Breakspear, M. (2017). Consistency-based thresholding of the human connectome. *NeuroImage*, *145*, 118–129. https://doi.org/10.1016/j.neuroimage.2016.09.053

Rubinov, M., Ypma, R. J. F., Watson, C., & Bullmore, E. T. (2015). Wiring cost and topological participation of the mouse brain connectome. *Proceedings of the National Academy of Sciences*, *112*(32), 10032–10037. https://doi.org/10.1073/pnas.1420315112

Sato, T. K. (2021). Long-range connections enrich cortical computations. *Neuroscience Research*, *162*, 1–12. https://doi.org/10.1016/j.neures.2020.05.004

Schaefer, A., Kong, R., Gordon, E. M., Laumann, T. O., Zuo, X.-N., Holmes, A. J., Eickhoff, S. B., & Yeo, B. T. T. (2018). Local-Global Parcellation of the Human Cerebral Cortex from Intrinsic Functional Connectivity MRI. *Cerebral Cortex*, *28*(9), 3095–3114. https://doi.org/10.1093/cercor/bhx179

Scholtens, L. H., Schmidt, R., de Reus, M. A., & van den Heuvel, M. P. (2014). Linking Macroscale Graph Analytical Organization to Microscale Neuroarchitectonics in the Macaque Connectome. *Journal of Neuroscience*, *34*(36), 12192–12205. https://doi.org/10.1523/JNEUROSCI.0752-14.2014

Schröter, M., Paulsen, O., & Bullmore, E. T. (2017). Micro-connectomics: Probing the organization of neuronal networks at the cellular scale. *Nature Reviews Neuroscience*, *18*(3), 131–146. https://doi.org/10.1038/nrn.2016.182

Shinn, M., Hu, A., Turner, L., Noble, S., Preller, K. H., Ji, J. L., Moujaes, F., Achard, S., Scheinost, D., Constable, R. T., Krystal, J. H., Vollenweider, F. X., Lee, D., Anticevic, A., Bullmore, E. T., & Murray, J. D. (2023). Functional brain networks reflect spatial and temporal autocorrelation. *Nature Neuroscience*, *26*(5), 867–878. https://doi.org/10.1038/s41593-023-01299-3

Smith, R. E., Tournier, J. D., Calamante, F., & Connelly, A. (2015). SIFT2: Enabling dense quantitative assessment of brain white matter connectivity using streamlines tractography. *NeuroImage*, *119*, 338–351. https://doi.org/10.1016/j.neuroimage.2015.06.092

Song, H. F., Kennedy, H., & Wang, X.-J. (2014). Spatial embedding of structural similarity in the cerebral cortex. *Proceedings of the National Academy of Sciences*, *111*(46), 16580–16585. https://doi.org/10.1073/pnas.1414153111

Sporns, O., & Betzel, R. F. (2016). Modular Brain Networks. *Annual Review of Psychology*, *67*(1), 613–640. https://doi.org/10.1146/annurev-psych-122414-033634

Sydnor, V. J., Larsen, B., Bassett, D. S., Alexander-Bloch, A., Fair, D. A., Liston, C., Mackey, A. P., Milham, M. P., Pines, A., Roalf, D. R., Seidlitz, J., Xu, T., Raznahan, A., & Satterthwaite, T. D. (2021). Neurodevelopment of the association cortices: Patterns, mechanisms, and implications for psychopathology. *Neuron*, 1–27. https://doi.org/10.1016/j.neuron.2021.06.016

Tian, Y., Margulies, D. S., Breakspear, M., & Zalesky, A. (2020). Topographic organization of the human subcortex unveiled with functional connectivity gradients. *Nature Neuroscience*, *23*(11), 1421–1432. https://doi.org/10.1038/s41593-020-00711-6

van den Heuvel, M. P., Bullmore, E. T., & Sporns, O. (2016). Comparative Connectomics. *Trends in Cognitive Sciences*, *20*(5), 345–361. https://doi.org/10.1016/j.tics.2016.03.001

van den Heuvel, M. P., Kahn, R. S., Goñi, J., Sporns, O., & Heuvel, M. P. V. D. (2012). High-cost, high-capacity backbone for global brain communication. *Proceedings of the National Academy of Sciences*, *109*(28), 11372–11377. https://doi.org/10.1073/pnas.1203593109

van den Heuvel, M. P., Scholtens, L. H., Feldman Barrett, L., Hilgetag, C. C., & de Reus, M. A. (2015). Bridging Cytoarchitectonics and Connectomics in Human Cerebral Cortex. *Journal of Neuroscience*, *35*(41), 13943–13948. https://doi.org/10.1523/JNEUROSCI.2630-15.2015

van den Heuvel, M. P., & Sporns, O. (2011). Rich-club organization of the human connectome. *The Journal of Neuroscience : The Official Journal of the Society for Neuroscience*, *31*(44), 15775–15786. https://doi.org/10.1523/JNEUROSCI.3539-11.2011

van den Heuvel, M. P., & Sporns, O. (2013). Network hubs in the human brain. *Trends in Cognitive Sciences*, *17*(12), 683–696. https://doi.org/10.1016/j.tics.2013.09.012

Vértes, P. E. (2023). Computational Models of Typical and Atypical Brain Network Development. *Biological Psychiatry*, *93*(5), 464–470. https://doi.org/10.1016/j.biopsych.2022.11.012

Vértes, P. E., Alexander-Bloch, A. F., Gogtay, N., Giedd, J. N., Rapoport, J. L., & Bullmore, E. T. (2012). Simple models of human brain functional networks. *Proceedings of the National Academy of Sciences*, *109*(15), 5868–5873. https://doi.org/10.1073/pnas.1111738109

Watts, D. J., & Strogatz, S. H. (1998). Collective dynamics of'small-world' networks. *Nature*, *393*(6684), 440–442. https://doi.org/Doi 10.1038/30918

Wei, Y., Scholtens, L. H., Turk, E., & van den Heuvel, M. P. (2019). Multiscale examination of cytoarchitectonic similarity and human brain connectivity. *Network Neuroscience*, *3*(1), 124–137. https://doi.org/10.1162/netn_a_00057

Zhang, X., Braun, U., Harneit, A., Zang, Z., Geiger, L. S., Betzel, R. F., Chen, J., Schweiger, J. I., Schwarz, K., Reinwald, J. R., Fritze, S., Witt, S., Rietschel, M., Nöthen, M. M., Degenhardt, F., Schwarz, E., Hirjak, D., Meyer-Lindenberg, A., Bassett, D. S., & Tost, H. (2021). Generative network models of altered structural brain connectivity in schizophrenia. *NeuroImage*, *225*, 117510. https://doi.org/10.1016/j.neuroimage.2020.117510

Supplementary material for "Coming up short: generative network models fail to accurately capture long-range connectivity"

Stuart Oldham[1,2], Alex Fornito[2] & Gareth Ball[1,3]
1. Developmental Imaging, Murdoch Children's Research Institute, The Royal Children's Hospital Melbourne
2. The Turner Institute for Brain and Mental Health, School of Psychological Sciences and Monash Biomedical Imaging, Monash University, Clayton, Australia
3. Department of Paediatrics, University of Melbourne, Melbourne

Corresponding author
Dr Stuart Oldham
Developmental Imaging,
Murdoch Children's Research Institute
Parkville 3052 VIC
Australia
stuart.oldham@mcri.edu.au

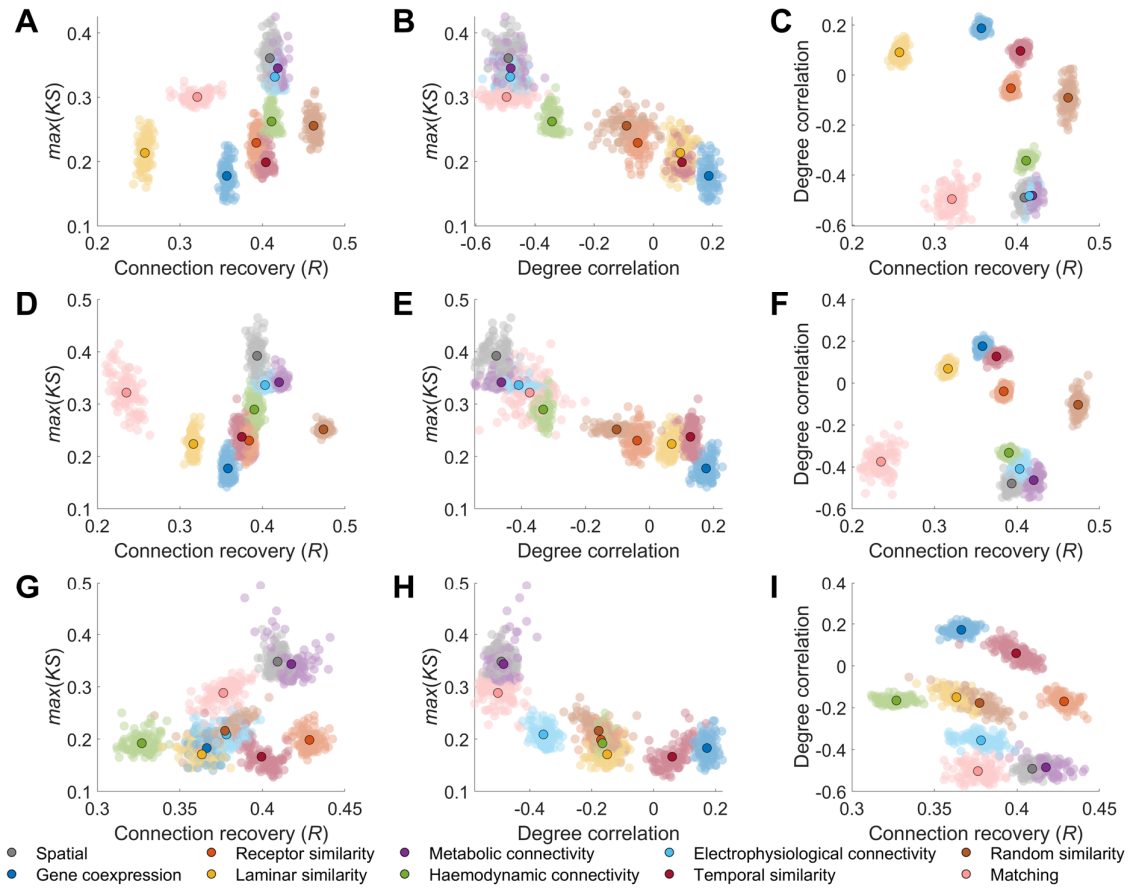

Figure S1. Performance of different formulations of generative network models in $\max(\mathbf{KS})$, connections recovered, and similarity of the degree distribution. Generative network models formulated using a multiplicative form and power-law distance decay $f(D_{ij}{}^{-\eta}) \times f(F_{ij}{}^{\gamma})$ showing the: **(A)** relationship between $\max(KS)$ and connections recovered; **(B)** relationship between $\max(KS)$ and the correlation between empirical and model degree; and **(C)** relationship between $\max(KS)$ and the correlation between empirical and model degree. Generative network models formulated using a multiplicative form and exponential distance decay $f(\mathrm{e}^{-\eta D_{ij}}) \times f(F_{ij}{}^{\gamma})$ showing the: **(D)** relationship between $\max(KS)$ and connections recovered; **(E)** relationship between $\max(KS)$ and the correlation between empirical and model degree; and **(F)** relationship between $\max(KS)$ and the correlation between empirical and model degree. Generative network models formulated using an additive form and power-law distance decay $f(D_{ij}{}^{-\eta}) + \alpha f(F_{ij}{}^{\gamma})$ showing the: **(G)** relationship between $\max(KS)$ and connections recovered; **(H)** relationship between $\max(KS)$ and the correlation between empirical and model degree; and **(I)** relationship between $\max(KS)$ and the correlation between empirical and model degree.

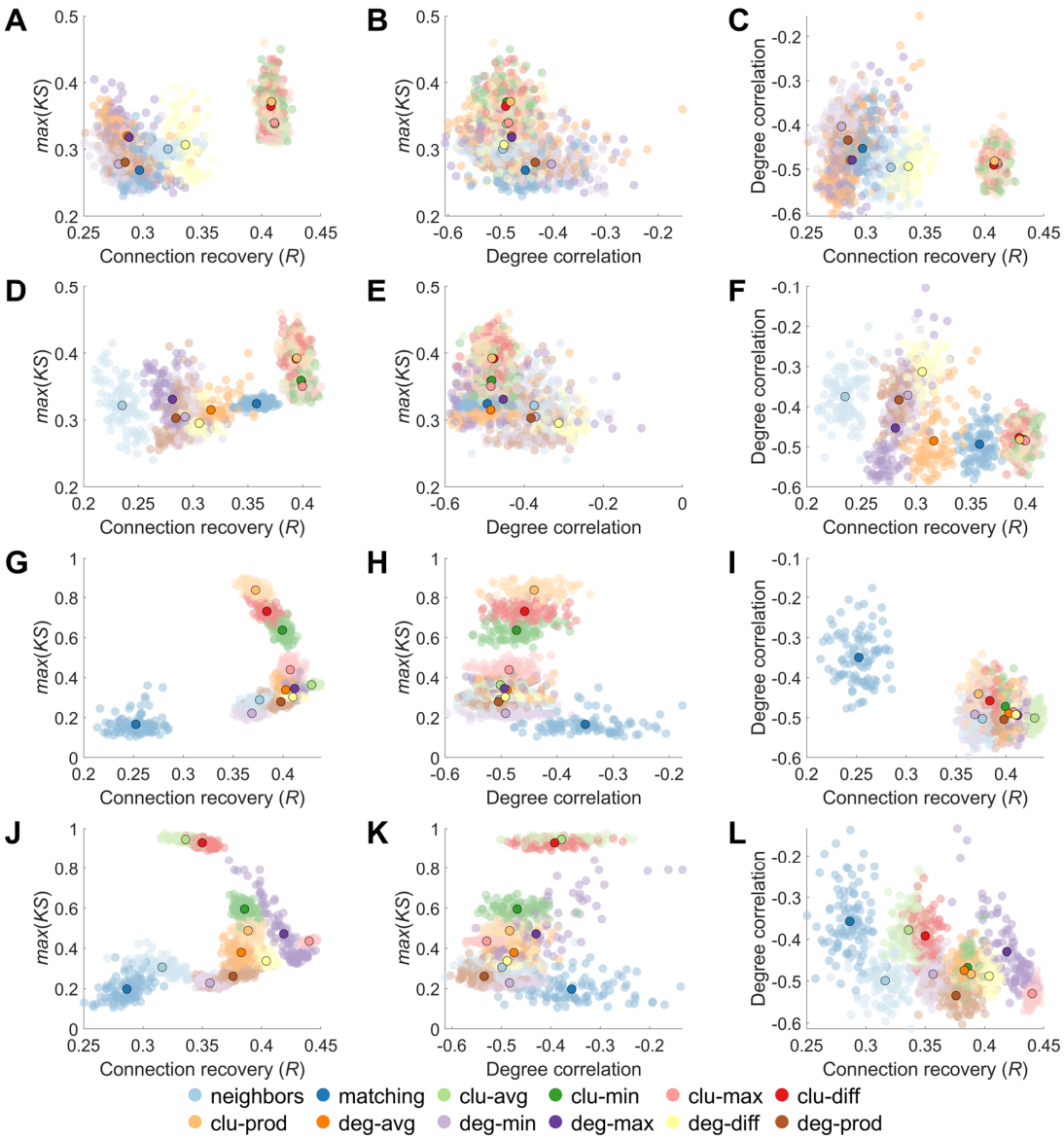

Figure S2. Performance of different topological generative network models in $\max(KS)$, connections recovered, and similarity of the degree distribution. Generative network models formulated using a multiplicative form and power-law distance decay $f(D_{ij}{}^{-\eta}) \times f(F_{ij}{}^{\gamma})$ showing the: **(A)** relationship between $\max(KS)$ and connections recovered; **(B)** relationship between $\max(KS)$ and the correlation between empirical and model degree; and **(C)** relationship between $\max(KS)$ and the correlation between empirical and model degree. Generative network models formulated using a multiplicative form and exponential distance decay $f(\mathrm{e}^{-\eta D_{ij}}) \times f(F_{ij}{}^{\gamma})$ showing the: **(D)** Relationship between $\max(KS)$ and connections recovered; **(E)** relationship between $\max(KS)$ and the correlation between empirical and model degree; and **(F)** relationship between $\max(KS)$ and the correlation between empirical and model degree. Generative network models formulated using an additive form and power-law distance decay $f(D_{ij}{}^{-\eta}) + \alpha f(F_{ij}{}^{\gamma})$ showing the: **(G)** relationship between $\max(KS)$ and connections recovered; **(H)** relationship between $\max(KS)$ and the correlation between empirical and model degree; and **(I)** relationship between $\max(KS)$ and the correlation between empirical and model degree. Generative network models formulated using an additive form and exponential distance decay $f(\mathrm{e}^{-\eta D_{ij}}) + \alpha f(F_{ij}{}^{\gamma})$ showing the: **(J)** Relationship between $\max(KS)$ and connections recovered; **(K)** relationship between $\max(KS)$ and the correlation between empirical and model degree; and **(L)** relationship between $\max(KS)$ and the correlation between empirical and model degree.

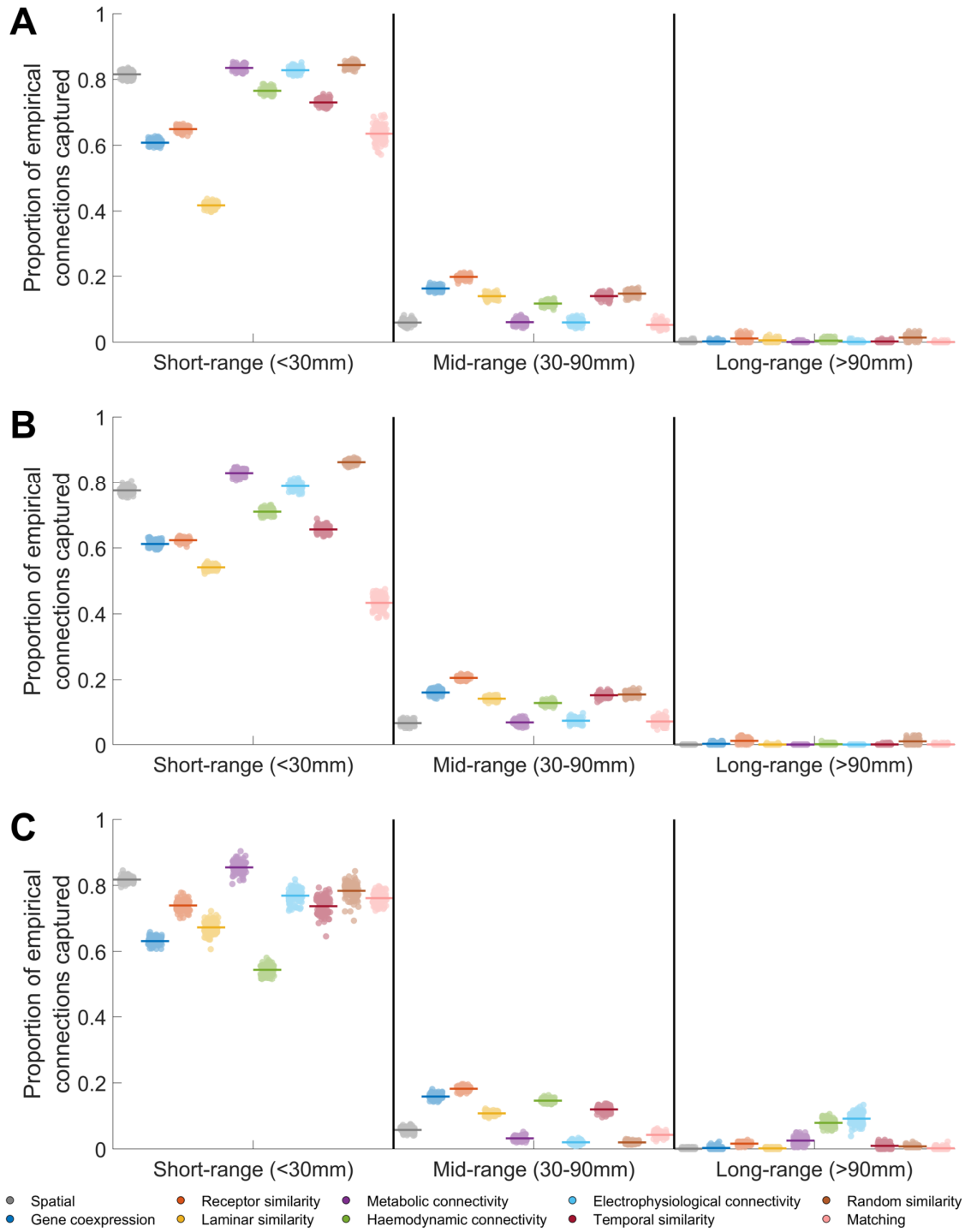

Figure S3. Connections captured at different distance thresholds for different generative network model formulations. Proportion of empirical short-range, mid-range, and long-range connections captured by the best fitting (lowest $\max(KS)$) generative network models for the: **(A)** multiplicative and power-law distance decay formulation $f({D_{ij}}^{-\eta}) \times f({F_{ij}}^{\gamma})$; **(B)** multiplicative and exponential distance decay formulation $f(\mathrm{e}^{-\eta D_{ij}}) \times f({F_{ij}}^{\gamma})$; **(C)** additive and power-law distance decay formulation $f({D_{ij}}^{-\eta}) + \alpha f({F_{ij}}^{\gamma})$. The coloured line indicates the average overlap, while each point indicates the result for an individual model network.

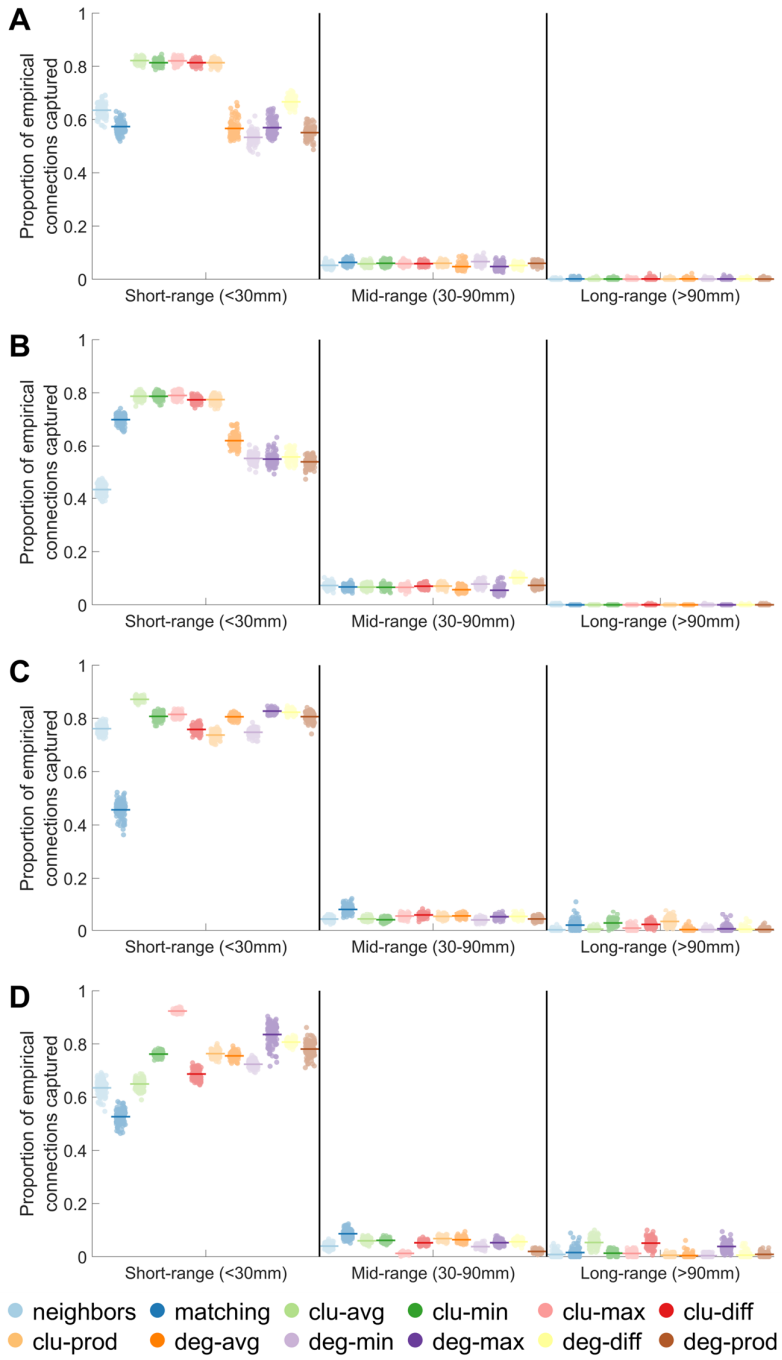

Figure S4. Connections captured at different distance thresholds for topological generative network models. Proportion of empirical short-range, mid-range, and long-range connections captured by the best fitting (lowest $\max(KS)$) topological generative network models for the: **(A)** multiplicative and power-law distance decay formulation $f({D_{ij}}^{-\eta}) \times f({F_{ij}}^{\gamma})$; **(B)** multiplicative and exponential distance decay formulation $f(\mathrm{e}^{-\eta D_{ij}}) \times f({F_{ij}}^{\gamma})$; **(C)** additive and power-law distance decay formulation $f({D_{ij}}^{-\eta}) + \alpha f({F_{ij}}^{\gamma})$; **(D)** additive and exponential distance decay formulation $f(\mathrm{e}^{-\eta D_{ij}}) + \alpha f({F_{ij}}^{\gamma})$. The coloured line indicates the average overlap, while each point indicates the result for an individual model network.

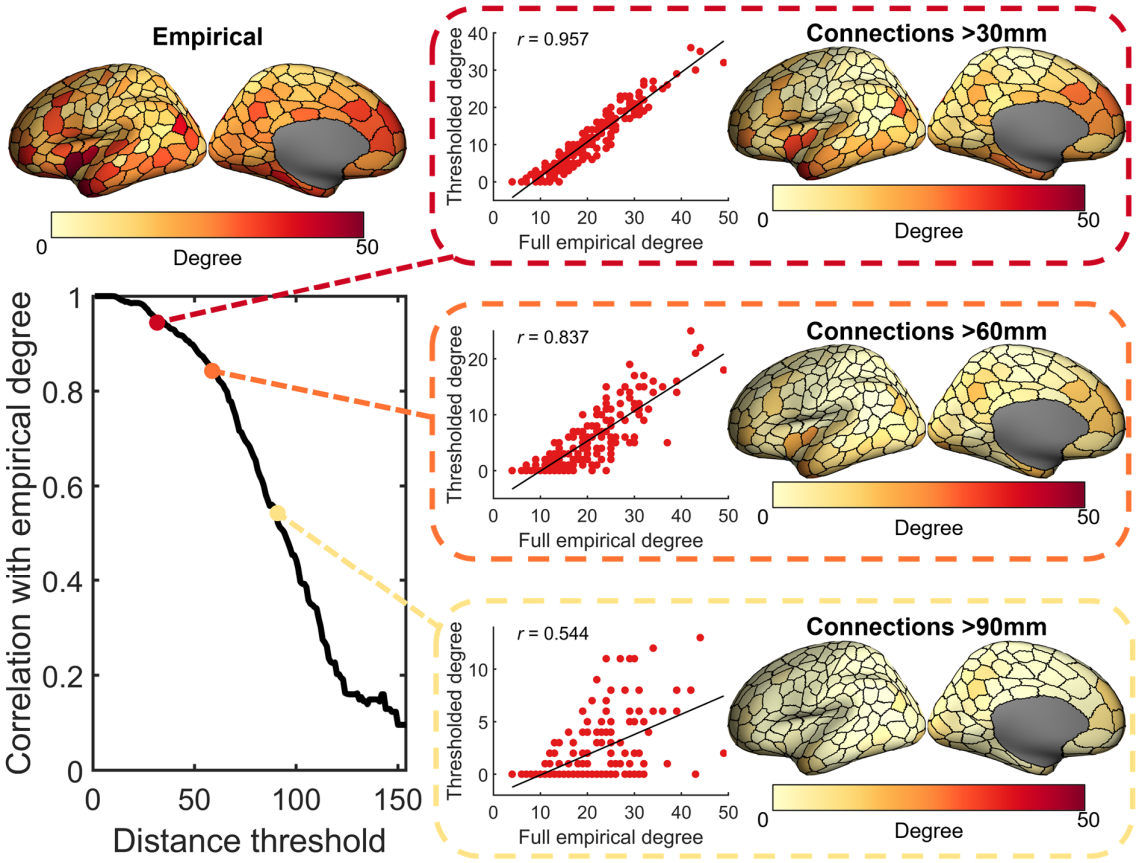

Figure S5. Similarity of the empirical degree sequence at different distance thresholds. Degree is calculated only using connections with a length greater than the current distance threshold. The thresholded degree is then correlated with the full empirical degree (i.e., degree calculated when using all empirical connections).

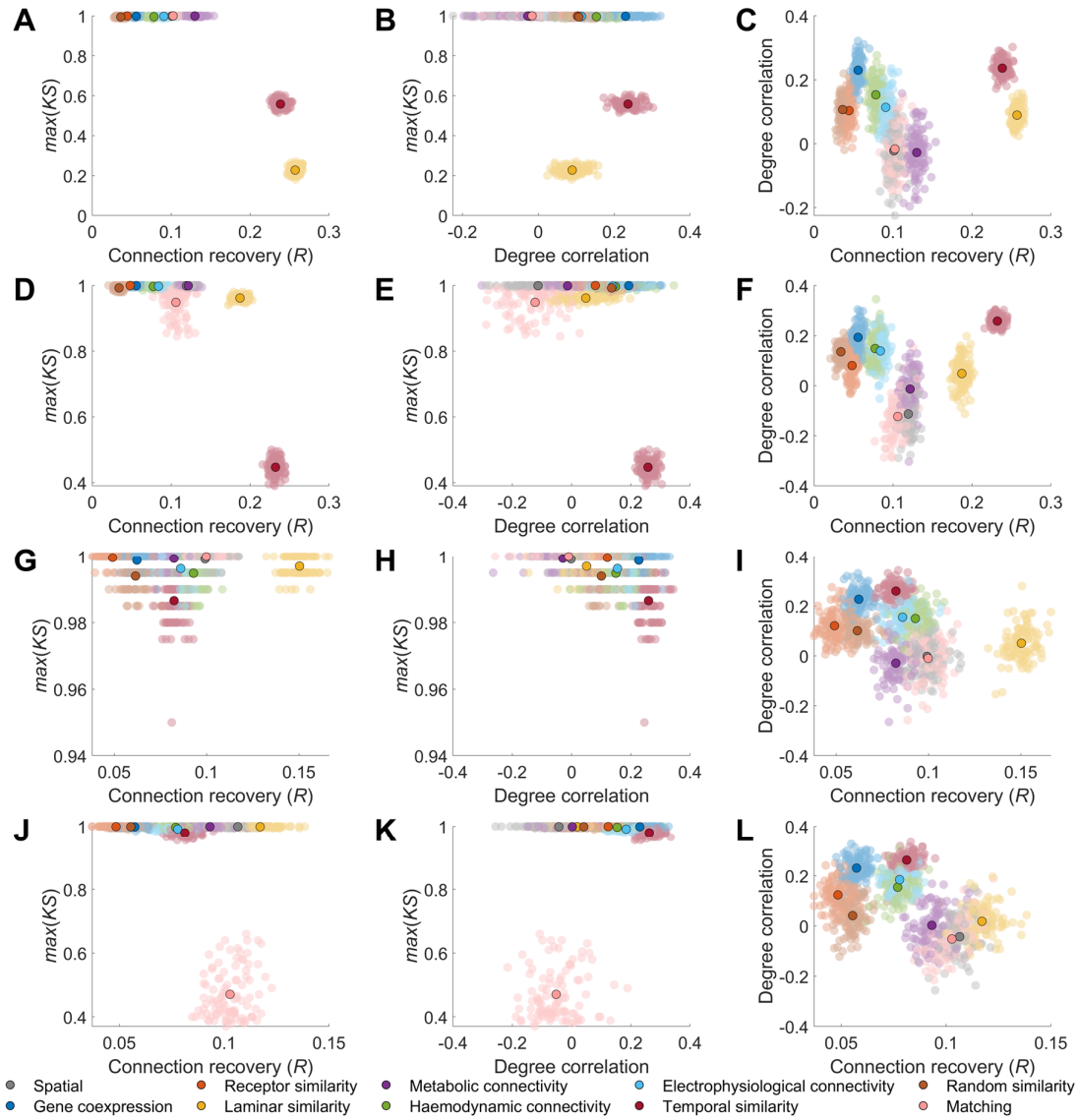

Figure S6. Analysis of generative network models with the strongest degree correlations, evaluated through $\max(KS)$, connections recovered, and degree correlation. (**A-C**) Models using a multiplicative form with power-law distance decay, $f(D_{ij}{}^{-\eta}) \times f(F_{ij}{}^{\gamma})$: (A) Relationship between $\max(KS)$ and connections recovered. (**B**) Relationship between $\max(KS)$ and the correlation between empirical and model degree. (**C**) Relationship between $max(KS)$ and the correlation between empirical and model degree. (**D-F**) Models using a multiplicative form with exponential distance decay, $f(\mathrm{e}^{-\eta D_{ij}}) \times f(F_{ij}{}^{\gamma})$: (**D**) Relationship between $\max(KS)$ and connections recovered. (**E**) Relationship between $\max(KS)$ and the correlation between empirical and model degree. (**F**) Relationship between $\max(KS)$ and the correlation between empirical and model degree. (**G-I**) Models using an additive form with power-law distance decay, $f(D_{ij}{}^{-\eta}) + \alpha f(F_{ij}{}^{\gamma})$: (**G**) Relationship between $\max(KS)$ and connections recovered. (**H**) Relationship between $\max(KS)$ and the correlation between empirical and model degree. (**I**) Relationship between $\max(KS)$ and the correlation between empirical and model degree. (**J-L**) Models using an additive form with exponential distance decay, $f(\mathrm{e}^{-\eta D_{ij}}) + \alpha f(F_{ij}{}^{\gamma})$: (**J**) Relationship between $\max(KS)$ and connections recovered. (**K**) Relationship between $\max(KS)$ and the correlation between empirical and model degree. (**L**) Relationship between $\max(KS)$ and the correlation between empirical and model degree.

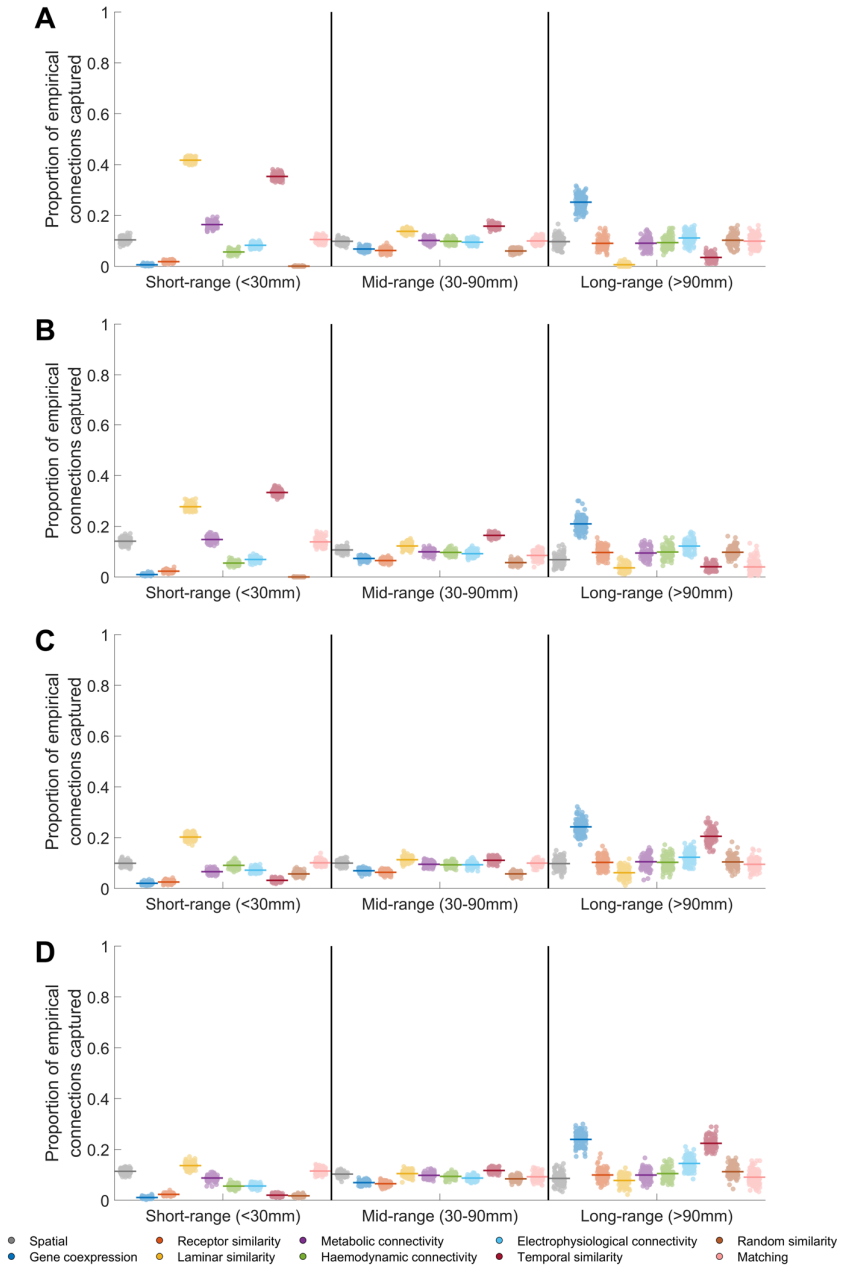

Figure S7. Connections captured at different distance thresholds for generative network models with the strongest degree correlations. Proportion of empirical short-range, mid-range, and long-range connections captured by the generative network models with the strongest degree correlations for the: **(A)** multiplicative and power-law distance decay formulation $f({D_{ij}}^{-\eta}) \times f({F_{ij}}^{\gamma})$; **(B)** multiplicative and exponential distance decay formulation $f(\mathrm{e}^{-\eta D_{ij}}) \times f({F_{ij}}^{\gamma})$; **(C)** additive and power-law distance decay formulation $f({D_{ij}}^{-\eta}) + \alpha f({F_{ij}}^{\gamma})$; **(D)** additive and exponential distance decay formulation $f(\mathrm{e}^{-\eta D_{ij}}) + \alpha f({F_{ij}}^{\gamma})$. The coloured line indicates the average overlap, while each point indicates the result for an individual model network.

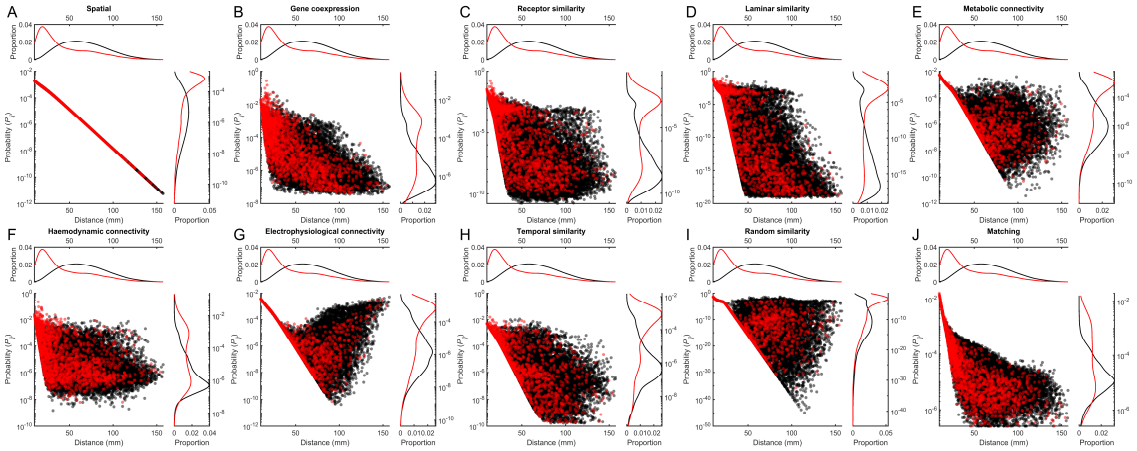

Figure S8. Connection probabilities in all generative network models. Shown are connection probabilities for the network with the lowest $\max(KS)$ for all GNMs. The connection probabilities are the mean probability assigned to each connection across all timepoints of the model. Red points indicate structural connections (i.e., connections that exist in the empirical data) while black points indicate non-structurally connected regions. Kernal density plots for the structural and non-structural connections are shown for the distributions of distance/length and probability against the respective axis.

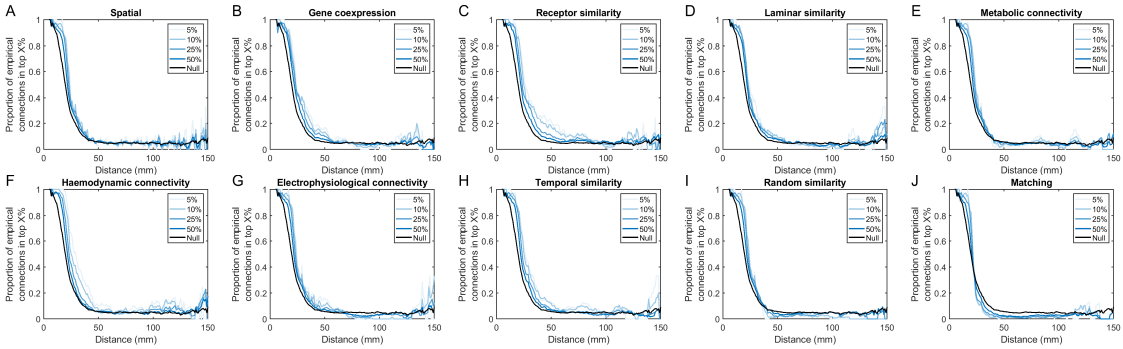

Figure S9. Most probable connections at different distances across generative network models. Using the sliding window analysis, at each distance the top X% of connections with the highest probability are found. The proportion of these which are empirical connections is then calculated. The "null" line indicates the proportion of empirical structural connections that exist at that distance (i.e., the probability of selecting an empirical structural connection if all connections at a given distance were equally probable).

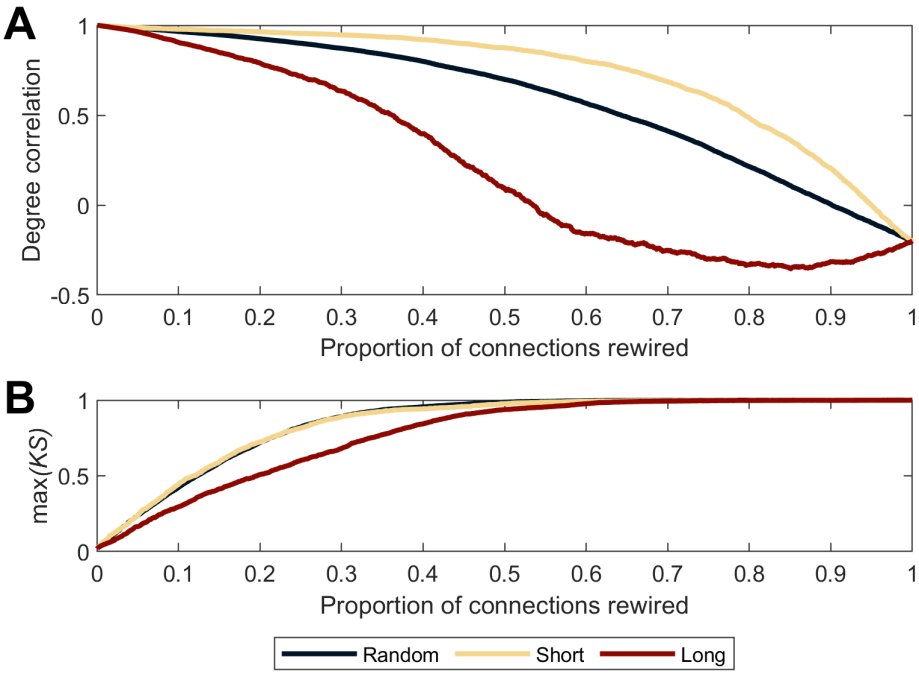

Figure S10. Effect of iteratively rewiring connections on the degree correlation. (A) The proportion of connections rewired and its effect on the degree correlation (i.e., correlation between node degree in the original and rewired network) for different rewiring algorithms. **(B)** The proportion of connections rewired and its effect on $\max(KS)$ for different rewiring algorithms. The *random* algorithm rewired connections at random but of a similar length; *short* rewired connections from shortest to longest connections with those of a similar length and; *long* rewired connections from longest to shortest connections with those of a similar length.

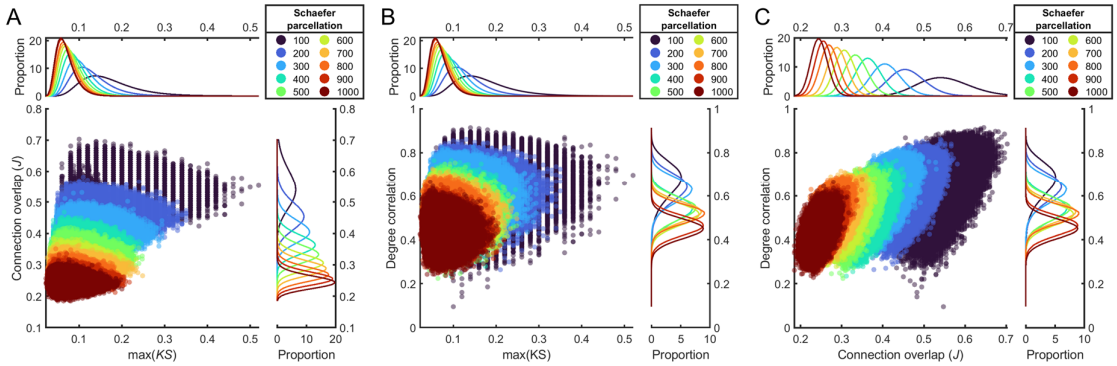

Figure S11. Performance of $\max(KS)$, connection overlap, and similarity of the degree distribution when comparing empirical networks produced using deterministic tractography. (A) Relationship between $max(KS)$ and connection overlap. **(B)** Relationship between $max(KS)$ and the correlation between two empirical networks nodal degree. **(C)** Relationship between connection overlap and the correlation between two empirical networks nodal degree. The kernel density plots show the distributions for each parcellation on the respective feature.

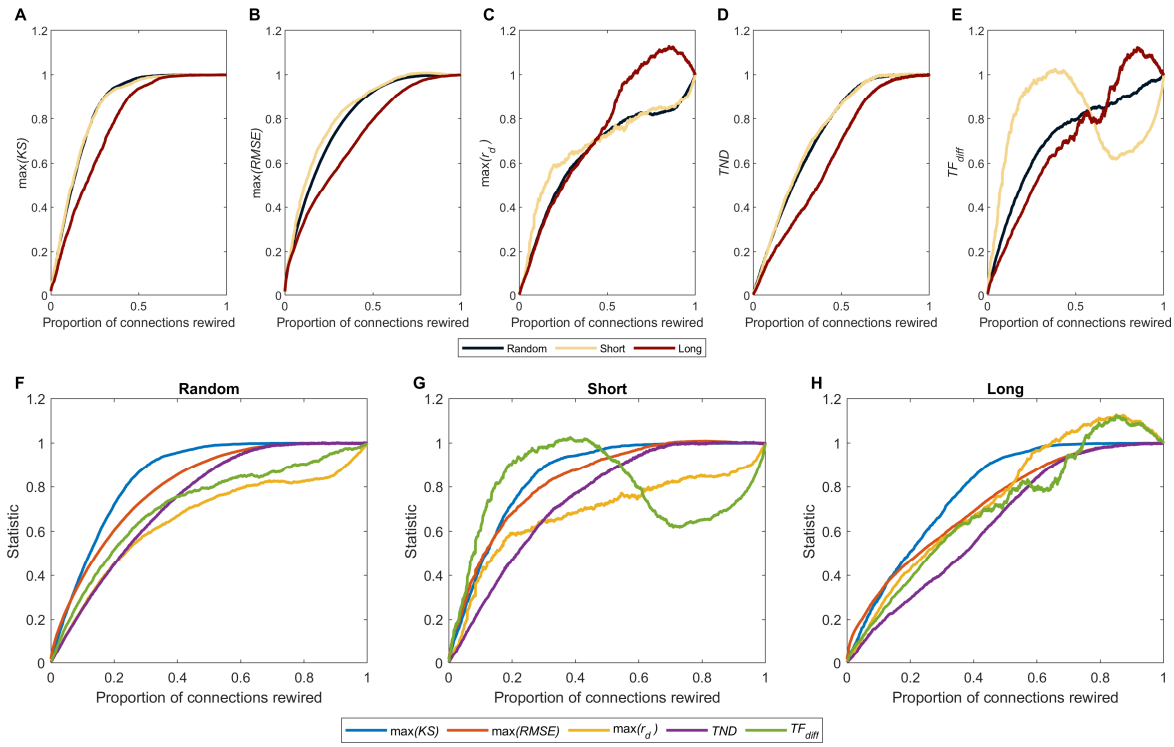

Figure S12. Effect of iteratively rewiring edges on different network similarity measures. The proportion of connections rewired and its effect on **(A)** $\max(KS)$; **(B)** $\max(RMSE)$; **(C)** $max(r_d)$; **(D)** TND; **(E)** and TF_{diff} for different rewiring algorithms. Each statistic has been normalised to its value obtained at 100% rewiring. Comparison of the different similarity measures for the: **(F)** *random*: **(G)** *short*; **(H)** *long*. The random algorithm rewired connections at random but of a similar length; *short* rewired connections from shortest to longest connections with those of a similar length; *long* rewired connections from longest to shortest connections with those of a similar length.

Table S1

Definitions of topological coupling terms

Name	F_{ij}	Description
clu-avg	$\left(\frac{c_i}{2}+\frac{c_j}{2}\right)$	Mean clustering coefficient of nodes i and j
clu-diff	$\lvert c_i - c_j \rvert$	Absolute difference between the clustering coefficients of nodes i and j
clu-max	$\max[c_i, c_j]$	Maximum clustering coefficient of nodes i and j
clu-min	$\min[c_i, c_j]$	Minimum clustering coefficient of nodes i and j
clu-prod	$c_i c_j$	Product of the clustering coefficients of nodes i and j
deg-avg	$\left(\frac{k_i}{2}+\frac{k_j}{2}\right)$	Mean degree of nodes i and j
deg-diff	$\lvert k_i - k_j \rvert$	Absolute difference between the degree of nodes i and j
deg-max	$\max[k_i, k_j]$	Maximum degree of nodes i and j
deg-min	$\min[k_i, k_j]$	Minimum degree of nodes i and j
deg-prod	$k_i k_j$	Product of the degrees of nodes i and j
matching	$\frac{2\sum_k A_{ik}A_{jk}}{k_i+k_j-2A_{ij}}$	The proportion of neighbors shared by nodes i and j
neighbors	$\sum_k A_{ik}A_{jk}$	The number of nodes neighboring both i and j

k_i = degree of node i, c_i = clustering coefficient of node i, A = adjacency matrix. Note that when topology was used in the model, to prevent undefined values from occurring (such as $F_{ij} = 0$) we add $\varepsilon = 10^{-6}$ to F_{ij}

Table S2

Different measures of network topological and topographical similarity

Network similarity measure	Formula	Definition
$\max(KS)$	$\max(\{KS_k, KS_c, KS_b, KS_e\})$	The maximum Kolmogorov-Smirnov (KS) statistic among: nodal degree k, clustering c, betweenness b, and edge connection length e
TND	$\sqrt{(\epsilon - \hat{\epsilon})^2 + \left(\Omega - \hat{\Omega}\right)^2 + \left(Q - \hat{Q}\right)^2 + \left(T - \hat{T}\right)^2}$	Euclidean distance between four global topological features: efficiency ϵ, diffusion efficiency Ω, modularity Q, transitivity T
TF_{diff}	$\sqrt{\sum_i \sum_j \left(TF(A)_{ij} - TF\left(\hat{A}\right)_{ij}\right)^2}$	Frobenius/Euclidean norm of the difference between the topological correlation matrices TF of two networks (Akarca et al., 2022)
$\max(RMSE)$	$\max(\{RMSE_k, RMSE_c, RMSE_h, RMSE_d\})$	The maximum root-mean-square-error (RMSE) of degree, clustering, harmonic centrality, and nodal distance
$\max(r_d)$	$\max(\{r_d(k), r_d(c) r_d(b), r_d(d)\})$	The maximum Pearson's correlation distance r_d among: nodal degree k, clustering c, betweenness b, and nodal distance d
Connection recovery (R)	$\frac{\lvert A \cap \hat{A} \rvert}{\lvert A \rvert}$	Proportion of connections in $\hat{A}$ that overlap with those in A
Connection overlap (J)	$\frac{\lvert A \cap \hat{A} \rvert}{\lvert A \cup \hat{A} \rvert}$	Proportion of overlapping connections between A and $\hat{A}$ over the total number of unique connections present in either network

Note. The ^ symbol indicates either a secondary adjacency matrix, or a feature derived from that matrix. $TF(A)$ is a 6×6 matrix of the Pearson correlations between the nodal distributions of degree, clustering, betweenness, nodal distance, mean matching, and closeness for the adjacency matrix A. The RMSE of harmonic centrality was used instead of the RMSE for betweenness ($RMSE_b$) as $RMSE_b$ was consistently much higher than the other RMSE values and would cause the measure to become entirely driven by differences in nodal betweenness values.

Table S3

Network measures/miscellaneous equations

Measure	Formula	Definition
KS	$KS_F = \max_x\left(\left\|G(x) - \hat{G}(x)\right\|\right)$	The maximum discrepancy between the cumulative empirical distribution functions G and $\hat{G}$ (Dudley, 2015)
RMSE	$RMSE_x = \frac{\sqrt{\frac{1}{n}\sum_i^n (x_i - \hat{x}_i)^2}}{\langle x \rangle}$	The root-mean-square-error (RMSE) of feature x, normalised by the mean of x
Degree	$k_i = \sum_{j \neq i} A_{ij}$	Number of connections a node has
Clustering	$c_i = \frac{\sum_{j,k} A_{ij} A_{jk} A_{ki}}{k_i(k_i - 1)}$	Average number of pairs of neighbours of a node that are connected (Watts & Strogatz, 1998)
Betweenness	$b_i = \sum_{u \neq i, u \neq v, v \neq i} \frac{\rho_{uv}(i)}{\rho_{uv}}$	The number of shortest-paths a node takes part in (Freeman, 1977)
Nodal distance	$d_i = \frac{1}{k_i} \sum_j D_{ij} A_{ij}$	The mean length of a node's connections
Harmonic (closeness) centrality	$h_i = \frac{1}{N-1} \sum_i \frac{1}{L_{ij}}$	The average of inverse shortest path lengths (Latora & Marchiori, 2001; Marchiori & Latora, 2000)
Matching index	$M_{ij} = \frac{\sum_k A_{ik} A_{jk}}{k_i + k_j - 2A_{ij}}$	The proportion of identical connections of two nodes normalised by the total number of connections belonging to the two nodes
Shortest-path efficiency	$\epsilon = \frac{1}{N(N-1)} \sum_{i \neq j} \frac{1}{L_{ij}}$	The average length of the paths between all nodes (Latora & Marchiori, 2001)
Diffusion efficiency	$\Omega = \frac{1}{N(N-1)} \sum_{i \neq j} \frac{1}{H_{ij}}$	The average length of random-walks between all nodes (Goñi et al., 2013)
Modularity	$Q = \frac{1}{2E} \sum_{i,j} \left(A_{ij} - \frac{k_i k_j}{2E}\right) \delta(m_i, m_j)$	The proportion of connections that occur within modules relative to that expect if connections were placed randomly (Newman & Girvan, 2004)
Transitivity	$T = \frac{\sum_{i,j,k} A_{ij} A_{jk} A_{ki}}{\sum_i k_i(k_i - 1)}$	The number of closed triplets divided by the number of all possible triplets (Newman, 2003; Wasserman & Faust, 1994)

Note. $G(x)$ and $\hat{G}(x)$ are the proportion of values of the respective features G and $\hat{G}$ that are less than or equal to x; ρ_{uv} is the number of shortest/ geodesic paths between nodes u and v; $\rho_{uv}(i)$ is the number of shortest paths between nodes u and v which pass through node i; L_{ij} is the length of the shortest path between node i and j; H_{ij} is the mean-first passage time from node i to node j; E is the number of edges in the network; $\delta(m_i, m_j)$ is the Kronecker delta function which is equal to one if nodes i and j are part of the same module and zero otherwise. When calculating the RMSE for two empirical networks, given both x and $\hat{x}$ correspond to observed values, instead of dividing by $\langle x \rangle$, the numerator was divided by $\frac{\langle x \rangle + \langle \hat{x} \rangle}{2}$ as to consider the averages of both sets of empirical observations. The mean matching index of node i can be calculated as $\frac{1}{N}\sum_j M_{ij}$ to obtain a nodal measure of the index. For identifying modules, modularity maximisation was used.